3 Differential thermal analysis and differential scanning calorimetry

P.J. Haines and F.W. Wilburn

3.1 Introduction

When an organic chemical is prepared, it is checked against known materials for purity and stability. One of the easiest ways of doing this is to determine its melting point! *This cannot be done by TG, since it involves no mass change*! This also applies to solid–solid phase transitions and to some solid-state reactions. We therefore need a technique that identifies these transitions. Such a technique will give us a simple way of identifying and assessing the quality of materials that may be applied across a large range of substances, from polymers to metals.

The magnitude and direction of the heat change of the system is more difficult to measure accurately and requires the more elaborate apparatus of calorimetry. The techniques to be discussed in this chapter give an interface between very sophisticated precision calorimetry and the qualitative observations of melting points and heat changes.

3.2 Historical

The early work in studying the interplay of heat and chemical or physical changes was largely qualitative, but the experiments of Lavoisier and Laplace around 1780 allowed the measurement of the quantities of heat energy associated with changes of state and chemical reactions. Although their apparatus required large quantities of sample, was slow to use and of low accuracy, Lavoisier's work has earned him the soubriquet of 'the grandfather of thermochemistry' [1]

During the same period, Fourier worked out mathematical descriptions of transfer processes and he is responsible for many of the fundamental ideas and equations that describe heat transfer. The idea for Ohm's law defining resistance came from Fourier's work, and the compliment is

P. J. Haines, *Thermal Methods of Analysis*
© Springer Science+Business Media Dordrecht 1995

repaid in the use of the 'thermal analogue of Ohm's law' in some theories of thermal analysis [2].

The work of Joule in the nineteenth century led to a greater understanding of the relationship of heat and work, and of the laws governing electrical heating, which now underly much of thermal analysis, both in control of the furnaces and in some DSC apparati. Joule also pioneered the use of twin calorimeter vessels, one containing a reference and the other the substance under investigation [3]. Modern high-precision calorimetry apparatus can be large and complex and the calculations involve many corrections [4]. Nowadays, laboratories generally require the opposite of these: small samples, rapid experiments, simplicity of use and ease of obtaining results!

Le Chatelier is often credited with being the first to use a differential thermal technique when he compared the temperatures shown by two thermometers, one within a sample and one outside it, as they were all heated in an oil bath. He was able to record melting transitions and the behaviour of clay samples. He later worked with thermocouples and characterised clay minerals into categories [5].

Roberts-Austen [6] pointed out that if the difference in temperature

$$T_S - T_R = \Delta T$$

is plotted against temperature or time, then a very sensitive method of detecting changes and transitions is obtained. This identifies the technique of *differential thermal analysis* (DTA)

Various theories were proposed to relate the DTA signals obtained to the heat capacity and enthalpy changes of transitions and reactions occurring during heating, but these were not entirely satisfactory. In 1964 Watson *et al.* [7] announced a *differential scanning calorimeter* (DSC) for quantitative measurements. There are now two main types of DSC and the distinction between the various sensors and apparati is given later. It is recognised that DTA and DSC, properly used, can make accurate measurements of the temperatures of thermal events, can detect the exothermic or endothermic nature of the event, and that DSC can make good measurements of the heat changes that occur.

3.3 Definitions

The two techniques will be considered together, since they are frequently used to study the same phenomena (see [8]).

3.3.1 *Differential thermal analysis (DTA)*

A technique in which the *difference in temperature* between the sample and a reference material is monitored against time or temperature while the temperature of the sample, in a specified atmosphere, is programmed.

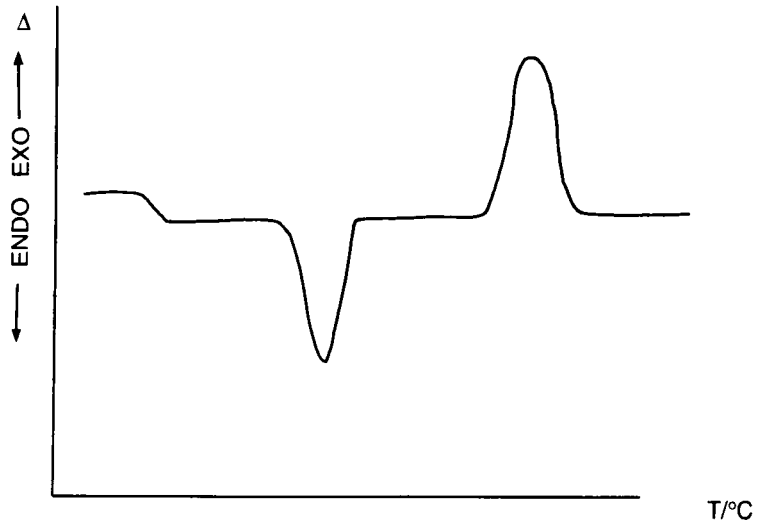

Figure 3.1 Typical DTA or DSC curve, using the convention that endothermic peaks go down. Δ indicates the differential signal for either temperature or power.

The DTA curve is generally a plot of the difference in temperature (ΔT) as the ordinate against the temperature T (or occasionally, time) as the abscissa. An *endothermic* event gives a *downward* 'peak' (Figure 3.1).

3.3.2 *Differential scanning calorimetry (DSC)*

A technique in which the *difference in heat flow* (power) to a sample (pan) and to a reference (pan) is monitored against time or temperature while the temperature of the sample, in a specified atmosphere, is programmed.

In practice, the heat is supplied to the sample contained in the pan, and similarly, to the reference in its pan.

Two types of DSC are recognised:

1. *Power-compensated DSC*, where the sample and reference are heated by separate, individual heaters, and the temperature difference is kept close to zero, while the difference in electrical power needed to maintain equal temperatures ($\Delta P = \mathrm{d}(\Delta Q)/\mathrm{d}t$) is measured.
2. *Heat flux DSC*, where the sample and reference are heated from the same source and the temperature difference ΔT is measured. This signal is converted to a power difference ΔP using the calorimetric sensitivity.

A constant calorimetric sensitivity is desirable, but not essential [9].

The DSC curve has ΔP as the ordinate and temperature (or occasionally, time) as the abscissa. Since an endothermic peak involves the absorption of *more* power by the sample, one convention plots endothermic peaks

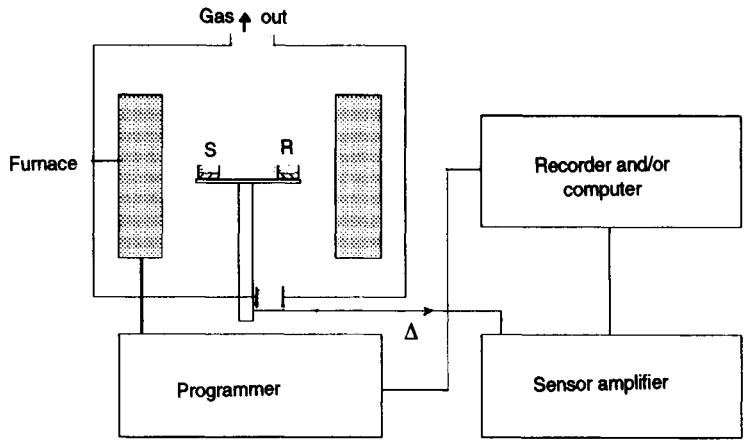

Figure 3.2 Schematic of a DTA or DSC apparatus. Δ indicates the differential signal.

upwards (Figure 3.1). This does cause some confusion, and in this text, we shall adopt the 'DTA' convention throughout, while indicating the sign of heat flow on the *y* axis.

3.4 Apparatus

The major parts of the system (Figure 3.2) are:

1. the DTA or DSC sensors plus amplifier
2. the furnace and its temperature sensor
3. the programmer or computer
4. the recorder, plotter or data acquisition device.

The range of designs for DTA and DSC is extremely wide, and shows a gradation from qualitative DTA to power-compensated DSC, as shown in Figure 3.3 [9].

3.4.1 *The sensors*

As shown in Figure 3.3, thermocouples are used as the sample and reference sensors for many DTA and DSC units. For low temperatures, copper–constantan or chromel–alumel have been used, while for higher temperatures, or more aggressive environments, Pt–Pt/13%Rh has been employed. Single thermocouples are in contact with the sample in ((a), (b)), but outside in types ((c)–(e)). Some Mettler and Setaram DSC units use multiple thermocouples or thermopiles ((d),(e)) to increase the signal. The 'Boersma' DTA, where the heat is conducted to the pans via a conducting metal disc, is used in several apparati.

The exceptional case is the power-compensated DSC (f), where the

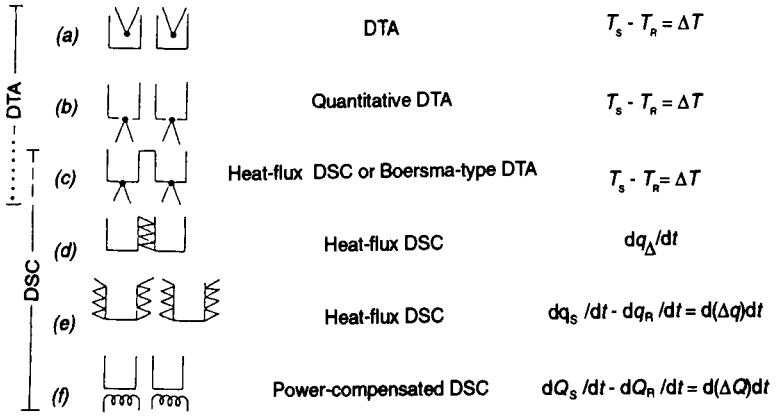

Figure 3.3 The DTA–DSC series. ⩚ , thermocouple; ⩚⩚⩚ , thermopile; ⌇⌇⌇ , heater [9].

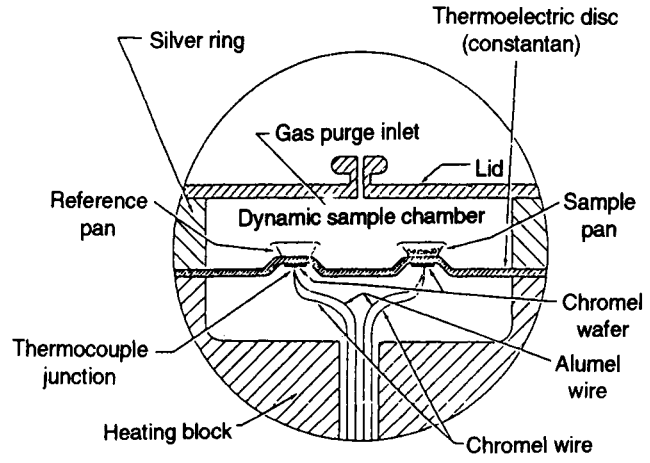

Figure 3.4 Heat flux DSC. (Courtesy TA Instruments Ltd.)

sensors are platinum resistors and the power is supplied to sample and reference separately.

Where the dividing line should be drawn between DTA and DSC is debatable [9], but several different manufacturers have shown [10] that their instruments satisfy the requirements of DSC by determining calorimetric data with good accuracy (Figures 3.4 and 3.5).

Pans and crucibles of many materials have been employed, but the majority of low-temperature instruments use aluminium pans and lids, provided they are not attacked by the samples and are only used well below the melting point of aluminium, 660 °C! For more aggressive environ-

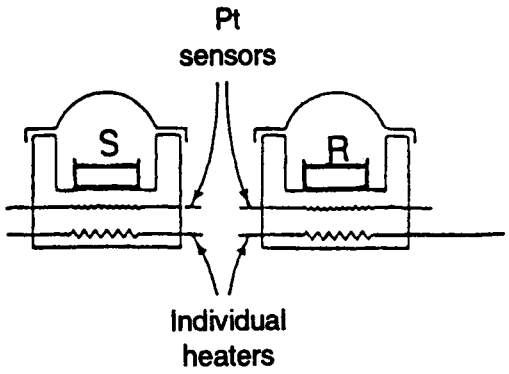

Figure 3.5 Power-compensated DSC. (Courtesy Perkin-Elmer Ltd.)

ments, platinum or ceramic crucibles may be used. The conductivity of the crucibles and their contact with the sensors affect the thermal analysis curves obtained.

A standard experiment might involve a sample of about 10–20 mg of powder, or a disc punched from a polymer film, or a bundle of fibres being placed in a weighed, lidded aluminium crucible, and the total mass recorded. Sometimes an inner liner is placed on top of the sample to enable the sample to make better contact with the base. The lid may be fixed to the base using a simple press, and can give a sealed crucible capable of withstanding about 2 atmospheres pressure. If vaporisation is not a problem, small pinholes can be punched in the lid to allow escape of gas products and reaction with the surrounding purge gas.

Special crucibles have been designed for containing higher pressures [11], or for mixing liquids [12], or for observing the sample during heating [13,14]. Liquids may be injected into the crucible using a syringe.

For the use of even higher pressures, the technique of *pressure DSC* (PDSC) has been invented. The entire DSC cell is enclosed in a strong stainless steel container capable of withstanding pressures from 1 Pa to 7 MPa (approximately 70 atm.). This means that reactions that produce high pressures of gases or react with gases under high pressure may be studied. Additionally, vaporisations may be suppressed by running at higher pressures. Uses of PDSC include the accelerated oxidative stability testing of materials such as oils under high pressures of oxygen [15] and the catalytic reduction of organic compounds with hydrogen [16].

3.4.2 *The furnace and controller*

Very similar comments can be made to those relating to TG (see p.28). For high-temperature DTA, large ceramic-lined, electrically heated furnaces

are used with electronic control. Many small DSC systems use a resistance-heated furnace enclosure of silver. The very high thermal conductivity of silver ensures that there is a uniform temperature. For the simplest DTA [17], a metal block, wound with an insulated heating element and having two wells for sample and reference cells and thermocouples, gives a satisfactory introduction to the principles of DTA.

Heating rates between 0 and 100 K/min are used, but the normal rate is about 10 K/min.

One extra feature is the use of DTA or DSC below room temperature. A cooling accessory or refrigeration unit is fitted around the cell and the whole is cooled directly with liquid nitrogen or other coolants. It is essential that dry purge gas is passed through the cell assembly during the cooling, since condensation of water or ice onto the cells might otherwise occur.

3.4.3 *The computer and display*

The need for computer control and rapid data processing is paramount with DSC, since the signal must be converted to the ΔP signal, using a calorimetric sensitivity stored in software, and the curves that are obtained must be analysed for thermal parameters by differentiation (to obtain onset temperatures, for example) and by integration (to obtain peak areas).

3.4.4 *The reference material*

Both DTA and DSC are defined as *differential* methods, where the behaviour of the reference material or pan is compared with that of the sample and its pan. We must take account of ALL the thermal properties that might be involved. For example, the emissivity of the sample may alter if it changes phase, or reacts, or changes colour [18]. This is often avoided by covering both sample and reference pans with snugly fitting lids, or by sealing them. In many cases, small samples may be run on a DSC against an empty pan as reference, but often better results are obtained by using an inert reference material of similar thermal properties in the reference crucible. For many applications, pure, dry pre-heated ('calcined') alumina, Al_2O_3, is satisfactory. Carborundum, SiC, has also been used.

Occasionally, to make the thermal properties of sample and reference more comparable, the sample may be diluted with the reference. It is obviously important that they should not react, and this dilution sometimes improves the baseline and peak shape in DTA experiments.

3.5 Theory of DTA and DSC (F.W. Wilburn)

The shape and size of a typical DTA or DSC curve is determined as much by the environment surrounding the sample and reference materials as by

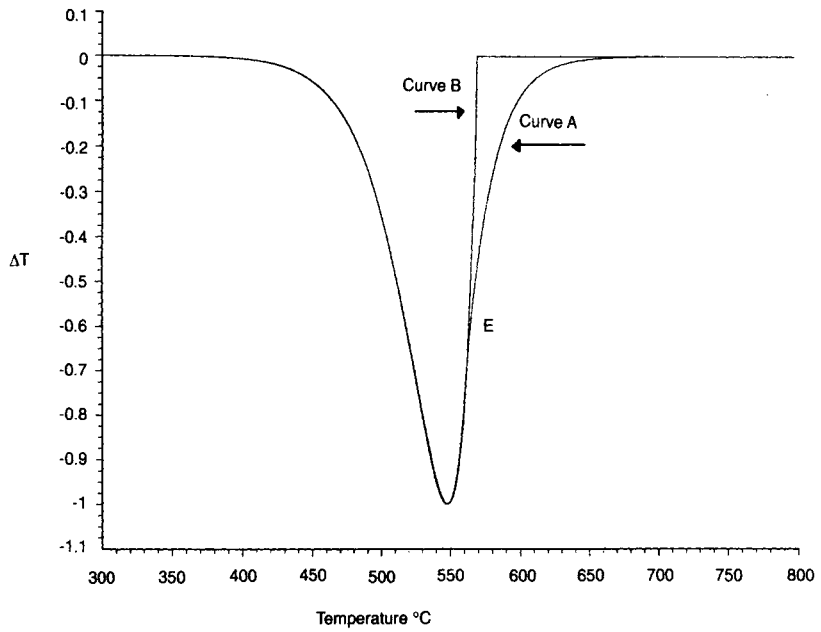

Figure 3.6 Typical DTA/DSC curves: A, practical curve; B, ideal curve.

the mechanism controlling the reaction and the sample material characteristics. Figure 3.6 shows a typical DTA or DSC curve for a material which melts (curve A) together with that (curve B) usually obtained in practical situations. During a melt, the reaction should end at the peak and the curve should then return abruptly to the baseline as in curve A. More often the curve obtained is that of curve B showing a relatively slow return to the baseline.

There are often further complications, in that the signal does not necessarily return to the *original* baseline, but to some other arbitrary baseline above or below this line, as shown in Figure 3.7. Indeed, the situation may be even more complicated, as when the baseline not only has a different value, but also a different slope. All these effects can be explained from the theory of DTA and DSC.

A full discussion of the theory of DTA and DSC would not only require this chapter, but this entire book, and even then it is questionable whether such information would be of use in answering some of the more usual questions asked when gaining information on typical DTA or DSC curves. It is the intention here to explain some of the more common variations seen in experimental curves in terms of theory and, where possible, to suggest ways of reducing errors due to such variations.

We shall first consider the theory of DTA and of the closely related *heat flux DSC*, and extend this to *power-compensated DSC* later.

Theories of DTA can usually be placed into one of two types.

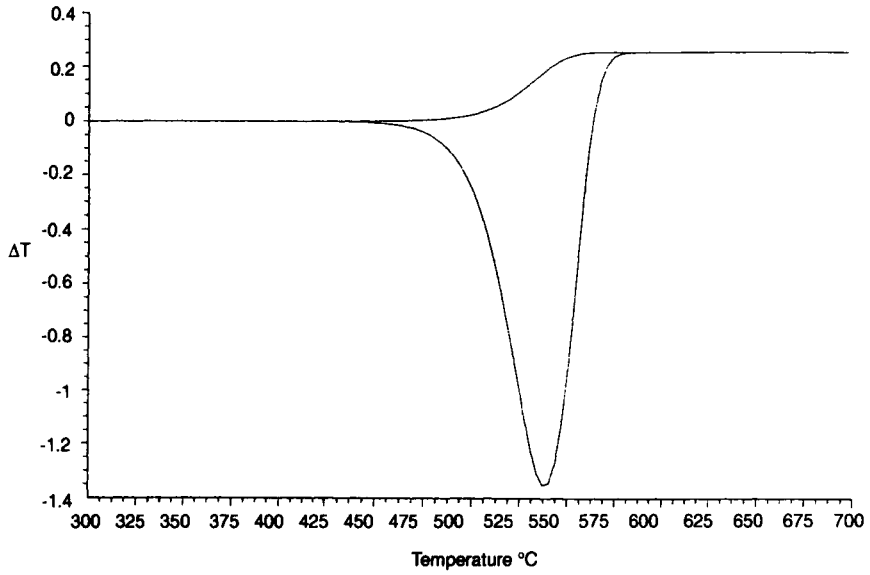

Figure 3.7 Difference temperature measured by thermocouples in the test materials when a change of sample thermal conductivity occurs.

In the first type, heat transfer equations such as the thermal analogue of Ohm's law:

$$dq/dt = (T_a - T_b)/R_{ab}$$

– where dq/dt is the heat flow between a and b and R_{ab} is their 'thermal resistance' – are developed but no account is taken of the reaction mechanism and the part it might play in the production of the peak. Further, for simplicity, it is generally assumed that the different parts of the apparatus (e.g. the sample holder) have no thermal gradients within themselves, which is not necessarily true.

In the second type, reaction equations such as those given by Brown [19] and Keattch and Dollimore [20] are manipulated to develop various relationships between the difference in temperature, ΔT, and the sample temperature at a specific time, from which it is claimed that activation energies and orders of reaction may be obtained. It is questionable whether such relationships are valid when heat transfer is taken into account. Some years ago, an electrical analogue of a DTA was developed [21–24] and was followed with a computer program which allowed heat transfer *and* reaction equations to be combined to show the influence of heat transfer on the shape of DTA curves and its effect on peak area.

Borchardt and Daniels [25] developed heat transfer equations for a system consisting of test tubes of liquid reactants within a stirred, heated liquid. In such a situation the transfer of heat to the test materials would be

rapid. Their theory, of the first type, is only valid if a number of limiting conditions are met:

1. The temperature in the holders must be uniform. While this would be true for liquids, it is not the case for solids.
2. Heat transfer must be by conduction only.
3. The heat transfer coefficient must be the same for both holders.
4. The heat capacity of the test materials must be the same.

All these conditions are relatively easy to achieve for liquids, due to the rapid transfer of heat within the system.

Coats and Redfern [26] adopted the second type of approach in that they manipulated reaction equations to show that various relations exist between the peak temperature and the heating rate from which it is possible to derive activation energies and 'orders of reaction'. No account was taken of heat transfer. Nearly all papers adopt one or other of these approaches.

Many earlier pieces of DTA apparatus were made mainly of refractory materials where heat transfer was comparatively slow. As might be expected resulting DTA curves from different apparati differed widely! One of the earliest papers on theory was that of Vold [27] who showed mathematically that there is a relationship between the 'active area' of a DTA curve and the heat involved. The 'active area' is that generated by the reaction itself, while the remaining area is that produced as ΔT returns to the baseline after the reaction has ceased (at point E in Figure 3.6). As this return is governed by natural cooling or heating, which is dependent on the thermal arrangement of the holder system, its form is exponential. Thus, a plot of $\ln(\Delta T)$ vs time for that part of the DTA curve beyond the peak becomes linear after point E. The area between the curve and its baseline from the commencement of the peak to the point E is the 'active area'. Further, Vold showed that the relationship between this 'active area' and the heat of reaction is:

$$\text{Heat} = A \cdot (\text{'active area'})$$

where A is the slope of the linear part of the $\ln(\Delta T)$–time curve. In this theory it was assumed that the physical properties of the sample and reference materials remained constant throughout the reaction. Thus, the shape of a DTA peak, particularly that portion at temperatures above the peak temperature, can be influenced by apparatus parameters. For reactions other than meltings, the assumption that the reaction ends before the DTA curve returns to the baseline is dependent on the type of reaction under investigation. The 'active' part of the DTA curve for melts, crystalline changes and zero-order reactions usually ends around the maximum of the DTA peak, so that the return to the baseline is exponential for a considerable portion of the DTA curve, and thus the end of the reaction can be defined fairly accurately as well as the A factor

referred to above. However, if the reaction is controlled by other types of mechanism then ΔT is often close to the baseline before the reaction ends. In this case it is difficult to determine the constant A. The high temperature end of a DTA curve can comprise a mixture of reaction mechanism and exponential return and can thus be different for different apparati.

The fact that this end of the DTA peak may not be a true representation of the reaction can have other consequences if two reactions follow in quick succession. In certain circumstances the two peaks may merge to produce a single peak. Indeed, this was used some years ago to test the discrimination ability of apparatus. A mixture of silica and potassium sulphate has two peaks, one the result of the structural inversion in silica at 573 °C, the other at 583 °C owing to a crystal transition in potassium sulphate. The ability to separate these peaks gave a measure of the resolution of the apparatus.

Many of the theories developed for the examination of DTA traces assumed that both before and after a reaction that produced a peak, the physical properties remained the same and were independent of temperature. On this assumption, the baseline remains the same across the DTA peak. However, there are very few practical DTA (or DSC) curves for which this is so. In older apparatus, the sample and reference temperatures were measured using thermocouples in the centre of the test materials (Figure 3.3(a)), which is the classsical DTA design. With such an arrangement, theory indicates that the position of the baseline is influenced by the relationship between the physical properties of the sample and reference materials. In order to maintain a constant, near-zero baseline, the physical properties such as the thermal conductivity k, heat capacity C and density ρ of sample and reference had to be closely matched. However, if any of these changed, either with reaction or with temperature, then the baseline of the DTA curve varied from zero, as shown in Figures 3.7 and 3.8. It can be shown that, for cylindrical samples of radius r, the equilibrium baseline offset ΔT is:

$$\Delta T = \{\beta \cdot r^2/4\} \cdot [(\rho_R \cdot C_R/k_R) - (\rho_S \cdot C_S/k_S)]$$

where β is the heating rate (K/s).

Usually the greatest change in any property of the sample material occurs during a reaction, so that it is not uncommon for the greatest baseline changes to occur during this period, i.e. during the production of a DTA peak. This change in baseline level affects the calculation of the area of the DTA peak. The magnitude of the error in calculation will depend on the size of the peak, a large peak being less affected than a small one. The error is compounded by not being able to define the 'true' baseline across the peak. The simplest expedient of drawing a straight line across the peak from the point where the DTA curve deviates markedly from the initial curve to a point where the curve returns to a level baseline nearly always results in an area that is too large, as shown in Figure 3.8. The baseline

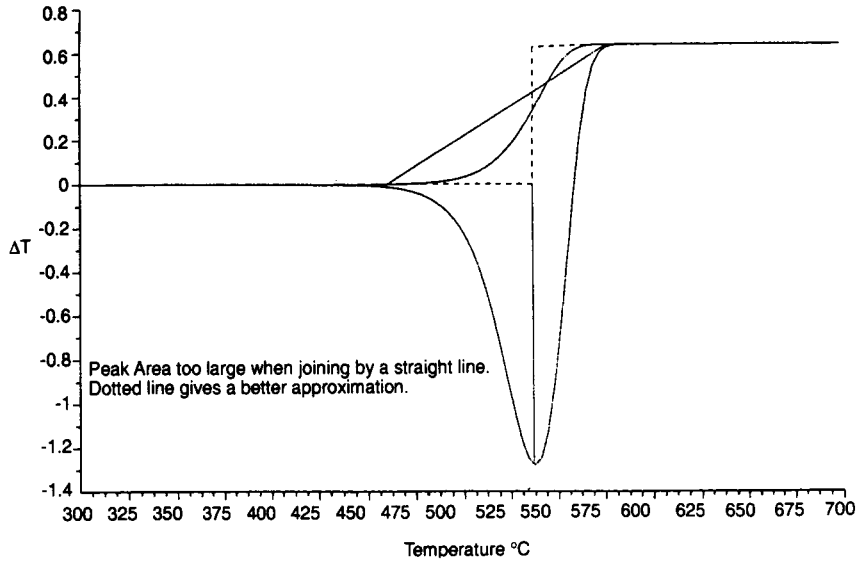

Figure 3.8 Difference temperature measured by thermocouples in the test materials when a change in sample specific heat capacity occurs.

change in Figure 3.8 was computed from preset changes in the physical constants occurring as the reaction was proceeding. It is sometimes possible to define a baseline across the peak in the situation when the level of the baseline is different before and after a peak, even if the true baseline cannot be defined easily [28], and this is shown as the dotted line in Figure 3.8. Much depends on the type of reaction involved and no general rule can be stated.

3.6 Heat flux DSC

If the measurement thermocouples are positioned beneath the sample and reference pans (Figure 3.3(c)–(e)) we have the heat flux DSC designs. The shift in baseline is now only influenced by changes in the sample specific heat capacity (Figures 3.9, 3.10) and is not affected by the other properties of the sample. Such a design of DSC may be used to measure specific heat capacities. Unfortunately, the change in baseline is also dependent on the characteristics of the pans holding the test materials so that the apparatus has to be calibrated using known standard materials.

The area under the peak is directly proportional to the heat of reaction [23,24,26].

$$\Delta H = K \int \Delta T \, dt = K \cdot (\text{peak area})$$

The calibration constant K converts peak area into joules, and is a *thermal factor* which may vary with temperature.

Problems of measurement of the area still arise owing to the difficulty in

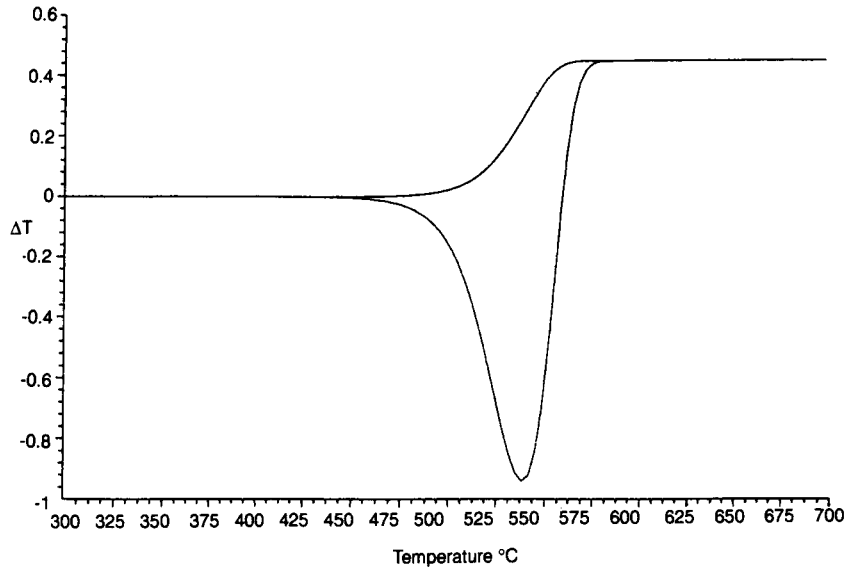

Figure 3.9 Difference temperature measured by thermocouples beneath the pan and test materials when a change in sample specific heat capacity occurs.

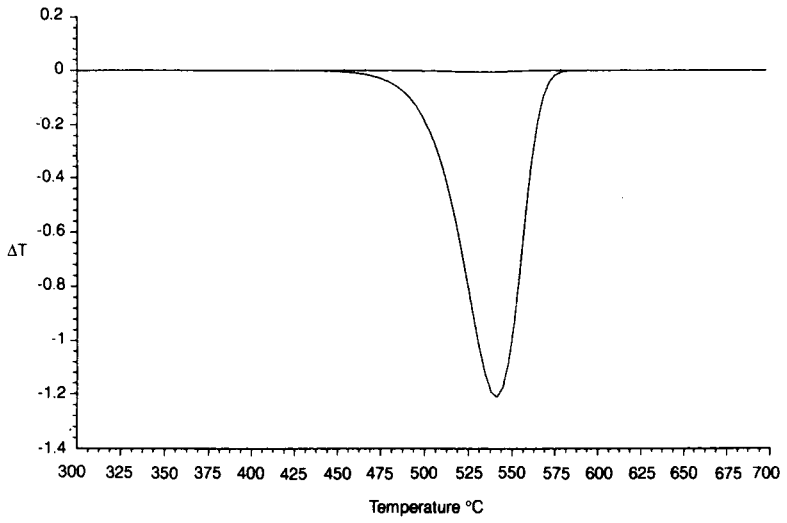

Figure 3.10 Difference temperature measured by thermocouples beneath the pan and test materials when a change in sample thermal conductivity or density occurs.

defining an accurate baseline. However, the DSC design does have some advantages (not least the reduction in chemical attack) over earlier DTA designs where the thermocouples were placed within the sample. Although the sensitivity is greater with the thermocouples within the sample, baseline shifts are often greater, being produced not only by changes in specific heat capacity but also by changes in thermal conductivity and density. In the DSC design, the positioning of the measuring thermocouples outside the test materials may reduce the sensitivity and overall response and some small inversions may not be seen when using certain types of DSC design.

3.7 Power-compensated DSC

In the other type of DSC, the sample and reference holders are insulated from each other and have their own individual sensors and heaters. The electrical circuitry operates to maintain the holders at the same temperature, within the electrical sensitivity of the circuitry, by varying the power supplied to the heater in each of the holders [29,30]. The thermal energy absorbed by the sample per unit time is exactly compensated by the differential electrical power ΔP supplied to the heaters. Measuring this power is equivalent to measuring the thermal power, and thus the baseline is:

$$\Delta P = \mathrm{d}\Delta q/\mathrm{d}t = \beta \cdot (C_S - C_R)$$

and the peak area gives ΔH directly. In power-compensated DSC the calibration constant required to convert peak area to joules is a constant *electrical* conversion factor.

3.7.1 *The effect of higher temperatures*

Most DSC designs developed for the measurement of specific heat capacity and ΔH are most suitable for temperatures up to around 700 °C. Above this, radiation, which is always present but increases with temperature, becomes significant. Most theories of DTA are based on heat transfer by conduction and assume that radiation is insignificant, and so are only relevant at lower temperatures. High-temperature cells tend to follow the DSC design to avoid thermocouple contamination at temperatures up to 1500 °C. However, at high temperatures heat transfer from the source of heat to the sample is rapid and if the measuring thermocouples are located beneath the pans, the sensitivity may be relatively low.

3.7.2 *Sample size*

When a sample is undergoing a reaction, there is, of necessity, a temperature gradient within it, as heat is abstracted (assuming an endo-

Table 3.1 Calibration materials for DTA and DSC [8, 30]

Material		Temperature (°C)	Enthalpy (J/g)
Cyclohexane	(t)	−83	
	(m)	7	
1,2-Dichloroethane	(m)	−32	
Phenyl ether	(m)	30	
Biphenyl	(m)	69.3	120.41
o-Terphenyl	(m)	58	
Polystyrene	(T_g)	105	
Potassium nitrate	(t)	128	
Indium	(m)	156.6	28.71
Tin	(m)	231.9	56.06
Potassium perchlorate	(t)	300	
Zinc	(m)	419.4	111.18
Silver sulphate	(t)	430	
Quartz	(t)	573	
Potassium sulphate	(t)	583	
Potassium chromate	(t)	665	
Barium carbonate	(t)	810	
Strontium carbonate	(t)	925	

Note. (t) = crystal transition; (m) = melting; Tg = glass transition temperature.

thermic change). To obtain meaningful calorimetric data, it is imperative that the sample size be kept to a minimum in order to reduce such gradients. However, if the sample consists of a number of materials, as in a study of reaction processes, then it is usually difficult to obtain a small, representative sample. In such a situtation, the ideal solution is to use a larger sample with the thermocouple embedded in it and to recognise that the apparatus is then only *qualitative* when used in this way.

3.8 Calibration

For accurate work, it is essential to calibrate the temperature scale, and for DSC instruments the apparatus must also be calibrated for calorimetric sensitivity. ICTAC have approved a set of standard substances, which are listed in Table 3.11 together with some other calibrants.

The particular instrument may have calibration factors already included in the computer software, but these must be checked from time to time. For a pure metal, such as 99.999% pure indium, the melting of which is shown in Figure 3.11, the extrapolated onset temperature T_e should correspond to the correct melting point of the metal, 156.6 °C. The integrated area of the peak A_S may then be used to calculate the calorimetric sensitivity constant K:

$$K = \Delta H_S \cdot m_S / A_S$$

where ΔH_S is the enthalpy of fusion of indium (28.71 J/g), m_S is the mass of sample of indium (g), A_S is the peak area (cm^2) and K is the calorimetric sensitivity (J/cm^2).

Note: If the area is calculated in K·s or W·s then obviously the units of K will change!

Calibration with several materials over the entire range of operation should enable the temperature dependence of K to be found.

Example *A sample of 6.68 mg of high purity indium gave a peak of area 21.94 cm^2. Calculate the value of K at 156 °C.*

$$K = (28.70 \times 6.68 \times 10^{-3})/\ 21.94 = 8.74 \times 10^{-3}\ \text{J/cm}^2$$

Comparison of the calorimetric calibration for one instrument, using a wide variety of materials over the range 0–660 °C [31], has shown that there is good agreement, provided samples are of reasonable size, and the heating rate is the same for calibration and measurement. The ICTAC committees on standardisation are continuously checking and reviewing the data and materials available for calibration [32].

A REMINDER!

The curves obtained for DTA and DSC will depend on the samples and instrument conditions used:

Sample:	chemical nature, purity, history.
Crucible:	material, shape.
Rate of heating	
Atmosphere:	gas, static, flowing.
Mass of sample:	volume, packing, distribution, dilution.

3.9 Applications

There are such a large number and variety of applications of DTA and DSC that readers should consult the journals or specialist texts for particular examples. The selection given below is representative of the range of uses of the techniques.

The applications may be divided roughly into two categories:

- *Physical changes and measurements*, such as melting, crystalline phase changes, changes in liquid and liquid crystalline states and in polymers, phase diagrams, heat capacity, and glass transitions, thermal conductivity and diffusivity and emissivity.
- *Chemical reactions* such as dehydrations, decompositions, polymer curing, glass formation and oxidative attack.

3.9.1 *Physical changes and measurements*

MELTING POINT AND ΔH_{fusion} OF MATERIALS

The determination of the melting point may be very easily done with simple apparatus, but ΔH of fusion is much more difficult to measure.

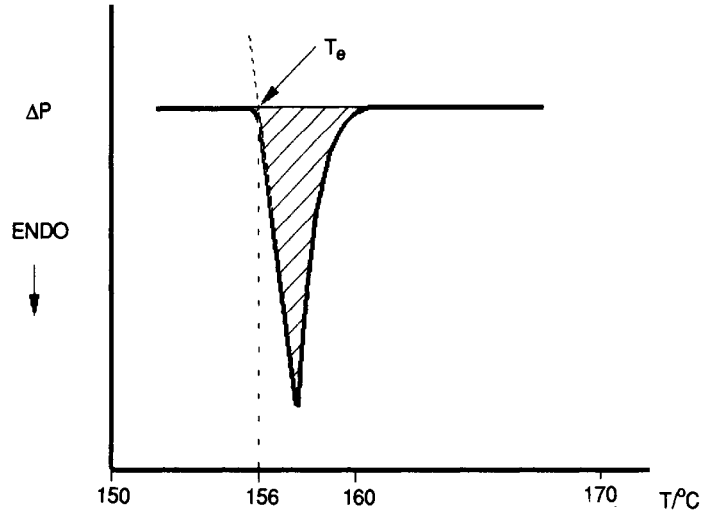

Figure 3.11 DSC peak for pure indium, showing the construction of the 'extrapolated onset' (6 mg, 10 K/min, nitrogen).

While DTA will give excellent qualitative measurements of T_m, we must use DSC for ΔH. Sharp melting peaks, similar to Figure 3.11, have been obtained, with suitable apparatus, over a very wide range of temperature, e.g. from *n*-heptane at −90 °C to palladium at 1550 °C. The melting points and ΔH of fusion of these compounds determined by DSC or DTA as the onset temperature are in good agreement with the literature values.

The crystallisation of pure materials can be awkward, since they often supercool past their true freezing point by many degrees.

CRYSTALLINE PHASE TRANSITIONS

The crystalline form of a compound can greatly affect its properties, such as solubility, density and electrical properties.

If a substance possesses two or more crystalline forms it is said to be *polymorphic*. If the forms are stable over particular temperature ranges, and have definite transition temperatures, the system is *enantiotropic*. If one form is stable but the other metastable over the whole range of temperature, then the system is *monotropic* and the less stable form will always be tending to transform to the more stable.

POTASSIUM NITRATE, KNO_3

Potassium nitrate shows rather complex behaviour when heated and cooled [31,32]. On first heating, there is an endothermic crystal transition

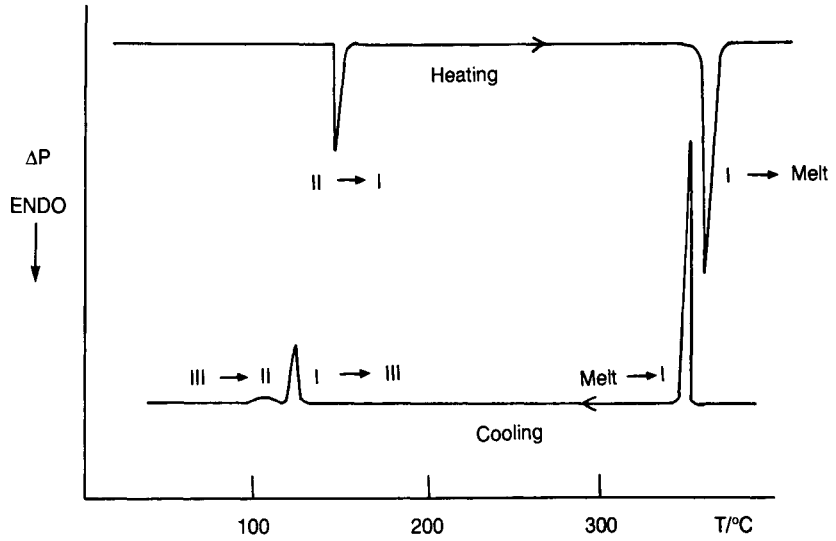

Figure 3.12 DSC curves for potassium nitrate (4 mg, 5 K/min, nitrogen).

(from form II to form I) at 128 °C with a ΔH of about 5.0 kJ/mol and a melting of form I at 334 °C with $\Delta H \sim 10$ kJ/mol. However, if the sample is then cooled from about 150 °C, we obtain an *exothermic* peak at 120 °C with ΔH of only −2.5 kJ/mol. This must mean that it is forming a *different phase. form III.* At lower temperatures it transforms slowly back to form II. These transformations are shown in Figure 3.12.

Other nitrates also show crystal phase transitions, especially rubidium nitrate [33], which has three transitions plus a melting, and ammonium nitrate which has four before melting. Since NH_4NO_3 is widely used as a fertiliser, and occasionally as an explosive, these have been extensively studied [34,35]. Figure 3.13 shows the DTA curve of ammonium nitrate.

First there is a small endotherm around 40 °C from form IV (rhombic II) to form III (rhombic I), followed by a second small endotherm at 80 °C transforming to form II (tetragonal). Two further, larger, endotherms follow at about 120 °C to form I (cubic) and at 170 °C to the melt. These transitions are very dependent on the treatment of the sample, and care must be exercised, since the *very* large exotherm following at about 200 °C represents explosion of the NH_4NO_3!

POLYMORPHISM IN FOODS AND PHARMACEUTICALS

Polymorphism is of particular importance in foods and pharmaceutical preparations, since it can affect the solubility, stability, physiological activity and bioavailability of the compound. As an example we shall

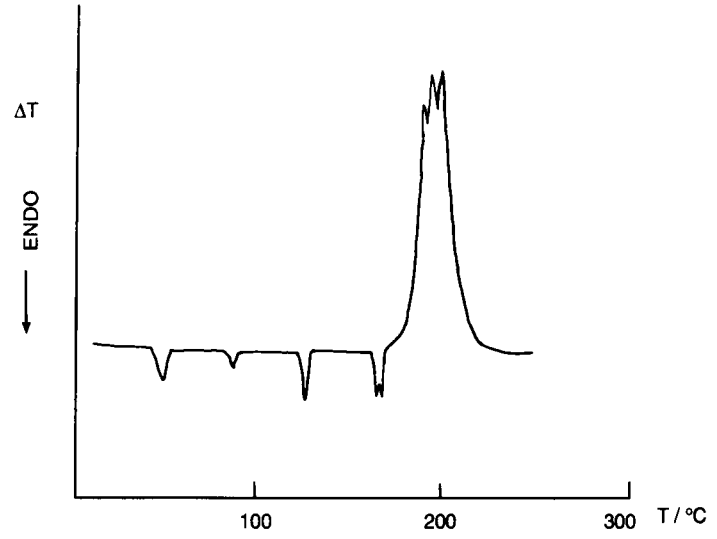

Figure 3.13 DTA curve for ammonium nitrate (powder, 10 mg, 10 K/min, static air).

consider the glycerides, esters of glycerol ($CH_2OH{\cdot}CHOH{\cdot}CH_2OH$) and long-chain aliphatic or unsaturated acids. They are present in fats, margarine and chocolate, and are used in many pharmaceutical preparations.

The polymorphism of glycerides has been reviewed by Chapman [36], who notes the use of microscopy, dilatometry, dielectric and X-ray diffraction studies in addition to thermal work and spectroscopy, and Aronhime [37] who concentrates on the applications of DSC. The glyceride systems show at least three phases, distinguished by their spectra and X-ray spacings. The highest melting β form is the most stable. The lowest melting α form and the intermediate β′ form are metastable with respect to the β form. Typical DSC traces are shown in Figure 3.14 for tristearin (glyceryl tristearate). On first heating of a sample rapidly cooled from the melt, we observe an initial melting of the α form at around 54 °C almost immediately followed by an exotherm due to the transformation and crystallisation of the stable β polymorph. The β form then melts at about 73 °C. If the liquid is then cooled to a temperature a few degrees above the melting point of the α polymorph, and held there until crystallisation occurs, the β′ polymorph is obtained. Heating this form produces a similar trace for the partial melting of β′, transformation to β and melting of β, as shown in the dashed curve of Figure 3.14. DSC studies have been made of the polymorphic changes in mixtures of confectionery fats [38] and of the thermal characterisation of edible oils and fats [39].

Polymorphism of pharmaceuticals is discussed fully in the book by Ford and Timmins [40] and by Hardy [41]. The forms of norfloxacin, a derivative of 4-quinolone carboxylic acid, were studied by DSC, TG, X-ray diffraction

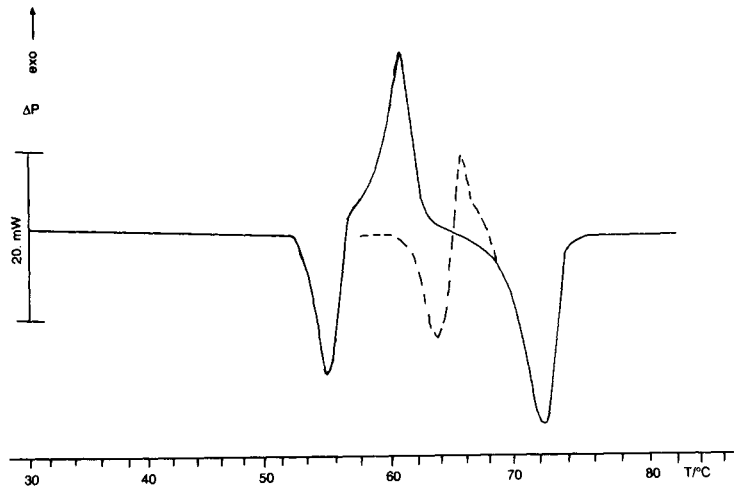

Figure 3.14 DSC curve for tristearin (4.3 mg, 5 K/min, nitrogen). Full line: first heat; dashed line: reheat from 57 °C.

and spectroscopy [42], showing the need to use *all* available analytical methods fully to characterise a material. Two different forms of this drug, A and B, which show a wide spectrum of antimicrobial activity, were obtained from different sources. The forms showed different X-ray patterns and gave the DSC traces in Figure 3.15 when heated in dry nitrogen at 10 K/min. The form A had a melting point of 219.5 ± 0.2 °C with a ΔH of 115 J/g, whereas form B also showed a broad transition at 195.6 ± 0.2 °C with a ΔH of 20 J/g which varied with heating rate. Since this transition was not seen on re-running the sample after cooling, the system is monotropic.

LIQUID CRYSTALLINE TRANSITIONS

The liquid crystalline state is of great importance in the preparation of display devices. Many types of liquid crystal phases are formed from molecules, often with polar end-groups, and with a rod-like structure. The liquid crystals represent various degrees of 'order' within the liquid. From a very ordered solid, we may progress to one of various *smectic* phases, which have plate-like order, or to a *nematic* phase, which has rod-like order, or to the *cholesteric* phase, which is a twisted nematic, and finally to the *isotropic*, completely disordered liquid [43,44].

Considering the order changes in these transitions, the greater the increase in *disorder*, the greater the entropy change ΔS. Since

$$\Delta S = \Delta H/T$$

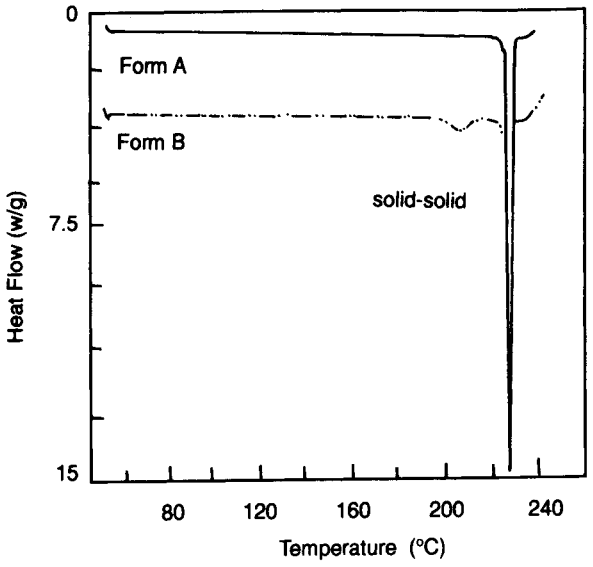

Figure 3.15 DSC curves for two polymorphic forms of norfloxacin. (Redrawn from [42].)

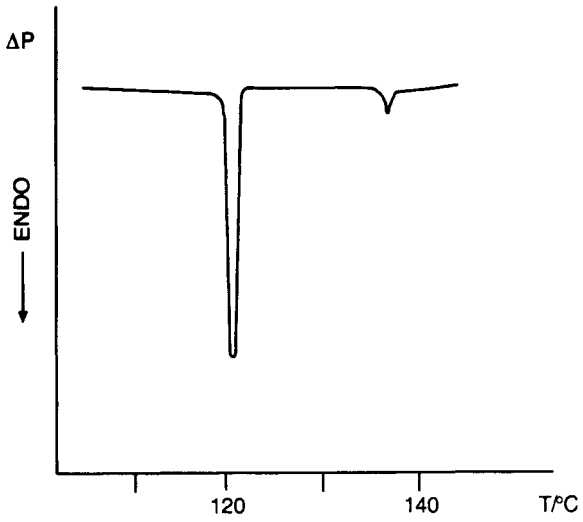

Figure 3.16 DSC curve for *p*-azoxyanisole (15 mg, 16 K/min, static air).

this means that ΔH will be large for a large change in order. Figure 3.16 shows the transformation of *p*-azoxyanisole

$$CH_3O{\cdot}C_6H_4{\cdot}N{=}NO{\cdot}C_6H_4{\cdot}OCH_3$$

The first transition at 119 °C has a large ΔH because the material goes

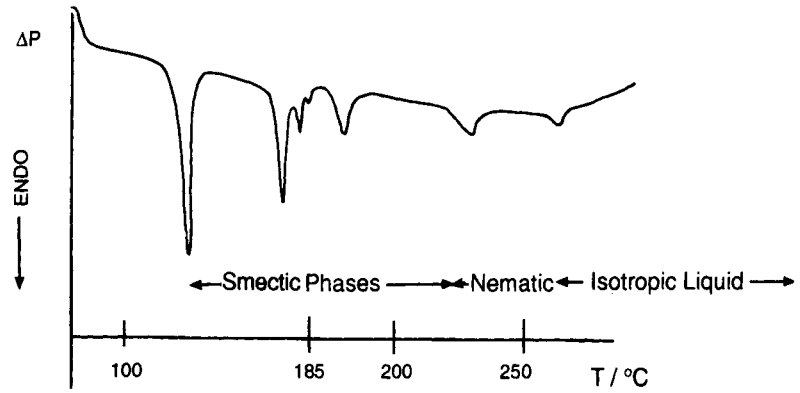

Figure 3.17 DSC curve for OOBPD (9 mg, 10 K/min, flowing nitrogen).

from ordered crystal to disordered, nematic liquid crystal. The second, smaller, transition at 135 °C goes to the true liquid phase.

Even more complex DSC curves are obtained for other systems, as shown in Figure 3.17, for *N,N'*-bis(4-octyloxybenzylidene)-*p*-phenylene diamine (OOBPD).

Exercise By examining the DSC trace of Figure 3.17, suggest probable answers to the following:

1. What is the most likely phase below 100 °C?
2. Given that the phase stable above 205 °C is a *nematic* liquid crystal, suggest the type of phase changes that give rise to the peaks between 120 and 205 °C.
3. On cooling this material to 80 °C, after all the liquid crystal phases have formed, *two exothermic* peaks are observed between 110 and 80 °C. What might be happening?

PHASE DIAGRAMS

When more than one chemical component is present, the thermodynamics become even more complicated, and the melting behaviour more complex. The traditional way of studying the phase behaviour of mixtures was by cooling curves, plotting T versus time as a mixture cooled from the melt [46]. DTA or DSC can give more information, more rapidly with smaller samples, provided sensible conditions are used – that is, fairly slow heating rates, preferably less than 10 K/min.

When a pure solid substance A does not dissolve at all in pure solid B, the freezing point of A is lowered by the presence of B, and the freezing point of B is lowered by A, giving the diagram shown in Figure 3.18. The

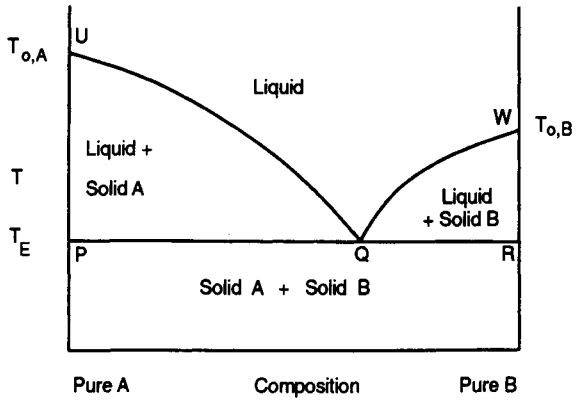

Figure 3.18 Eutectic phase diagram.

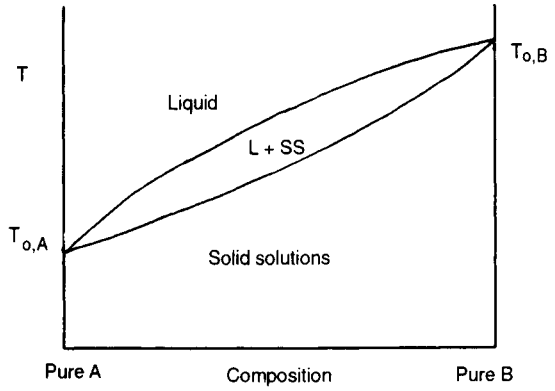

Figure 3.19 Phase diagram for a continuous series of solid solutions.

lowest temperature at which liquid can exist is called the *eutectic temperature* T_E and below this we have various mixtures of crystals of A and crystals of B.

When A and B are very similar in structure, for example, both form cubic crystals, they may form solid solutions, where a mixed crystal structure is obtained, having crystal lattice parameters intermediate between those of A and B. This gives the phase diagram shown in Figure 3.19 [47] or the phase diagram of Figure 3.20.

The DSC or DTA curve of any of the mixtures in these systems generally shows the phase changes.

When the temperature is higher than the solidus line, PQR, the mixture will start to melt and an endothermic peak will be obtained, whose size will depend upon the amount which melts at this temperature. The nearer the mixture is to the eutectic composition Q, the larger the peak at T_E. The

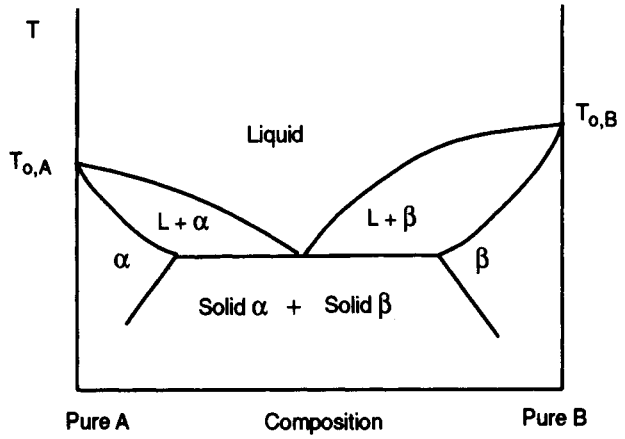

Figure 3.20 Phase diagram for a system with partially miscible solids α and β.

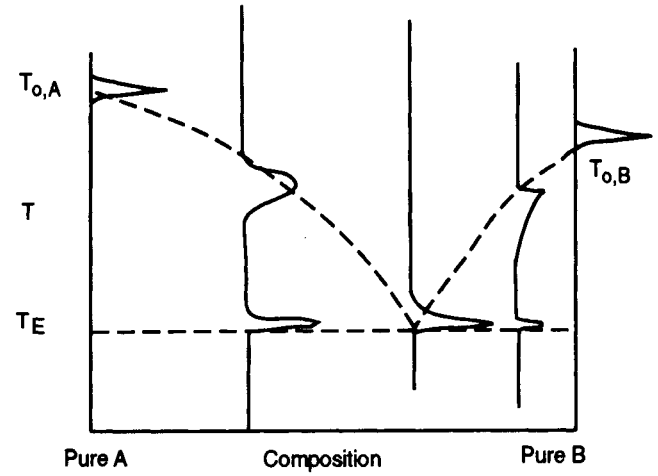

Figure 3.21 Eutectic phase diagram with superimposed DTA curves.

mixture will continue to melt, gradually, until the liquidus line UQW is reached, when the final fraction will become liquid. This temperature is given by the *final* peak of the trace.

Eutectic systems give two peaks, as shown in Figure 3.21. Solid solutions give a single, broad peak, as shown in Figure 3.22. Partially miscible systems give both sorts! When the components react to form compounds, this gives more complex diagrams [47] which may still be studied by thermal methods. The technique has been used extensively to study metallurgical phase diagrams [48,49], mixtures of liquid crystals [50] and pharmaceuticals [40].

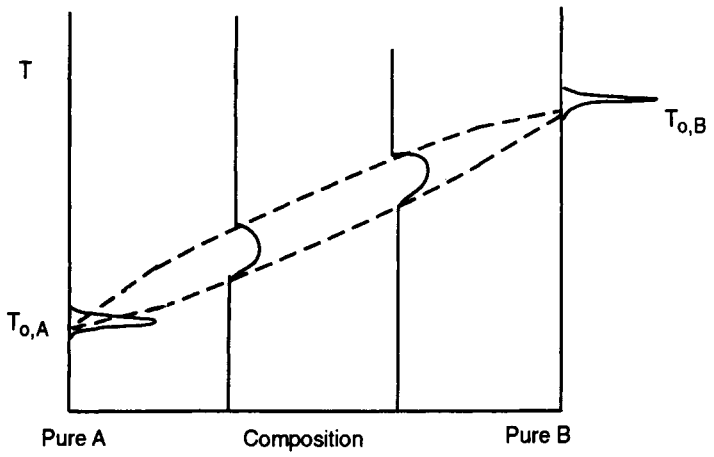

Figure 3.22 Solid solution phase diagram with superimposed DTA curves.

COMPATIBILITY OF PHARMACEUTICAL MIXTURES

This term implies that two or more components of a pharmaceutical dosage form may coexist without interaction during the whole shelf life of the preparation. Often the dosage form contains the active drug component plus other components or excipients to dilute, bind or disperse the drug. If there is physical or chemical interaction, then the physical and pharmaceutical properties of the mixture may be greatly affected. Jacobson and Reier [51] studied stearic acid mixtures with penicillins and showed that DSC methods correlated well with 8 week 50 °C stability tests. If there is no interaction, either physical or chemical, then the dosage mixture should show the same thermal analysis features as the original pure components, in the appropriate proportions. Any changes or new features indicate interaction, as shown in Figure 3.23. Grant *et al.* [52] showed that a mixture of glycerides showed eutectic behaviour, but that this was altered considerably when therapeutic amounts of ketoprofen were added.

Giordano *et al.* [53] showed that although a simple physical mixture of the drug trimethoprim (TMP) with the excipient cross-linked polyvinylpyrrolidone (PVP–XL) showed the same features as the original pure components, grinding the materials together changes the behaviour, as shown in Figure 3.24.

THERMOPLASTIC POLYMER PHASE CHANGES

Polymers which melt before they decompose may crystallise completely, or may remain as irregular, amorphous solids or glasses [54]. On heating a brittle 'glassy' polymer, the change to a more plastic material shows as an increase in heat capacity, as discussed below. The polymer molecules are

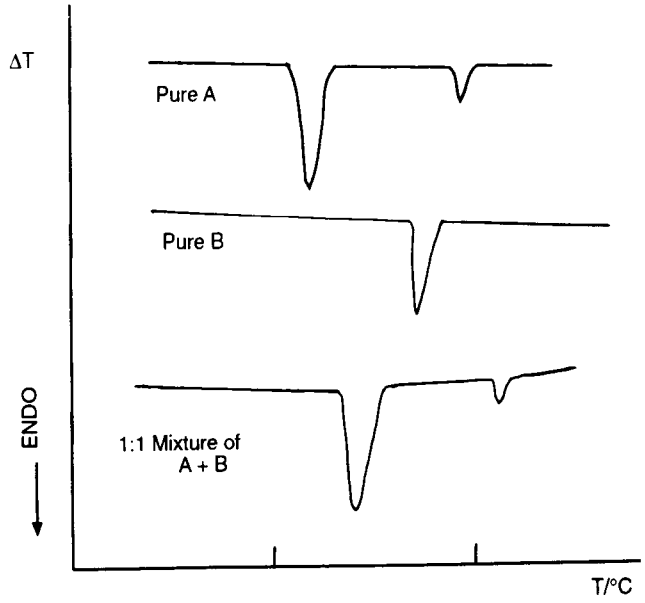

Figure 3.23 Schematic DTA curves for compatibility of materials.

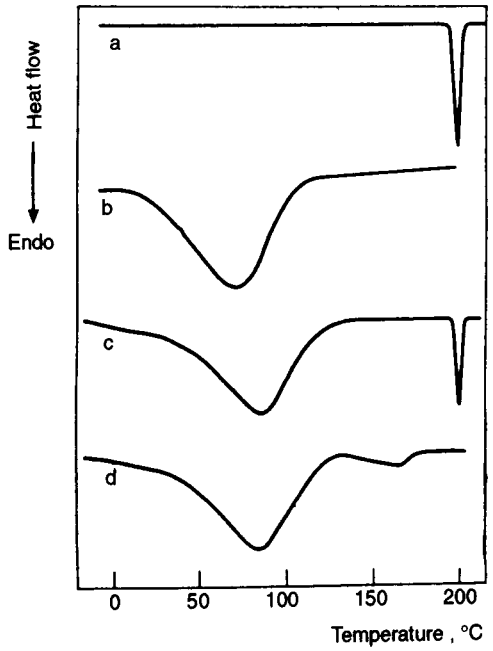

Figure 3.24 DSC traces of (a) PVP–XL (b) TMP, (c) physical mixture of 75% PVP–XL/ 25% TMP, (d) ground mixture of 75% PVP–XL/25% TMP [53].

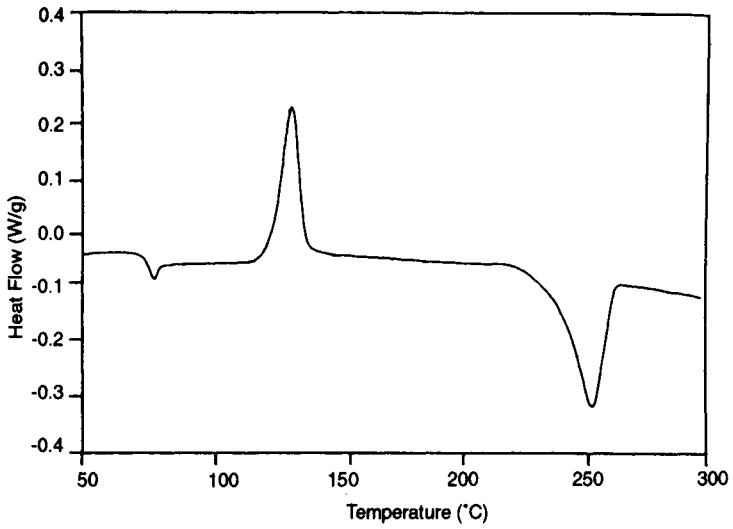

Figure 3.25 DSC curve for poly(ethylene terephthalate), PET, quenched from melt (10 mg, 10 K/min, flowing nitrogen).

then freer to move and can rearrange into the more regular structure of a crystal, giving an exothermic peak of 'cold crystallisation'. Finally, the crystalline polymer will melt to a liquid often over a broad range. With some polymers such as atactic polystyrene, this is difficult to detect. Figure 3.25 shows all these changes for poly(ethylene terephthalate), PET.

Some polymer samples can show multiple melting endotherms, indicating that portions of the sample have crystallised at different temperatures during the previous thermal treatment.

Polymeric samples often do not crystallise completely. The area of the melting peak of a partially crystalline sample may be compared to that of a standard of known crystallinity, or a completely crystalline sample, to give the percentage crystallinity [55].

$$\% \text{ Crystallinity} = \frac{\text{Area of sample melting peak} \times (\% \text{ Standard})}{\text{Area of standard melting peak}}$$

The components in polymer blends may melt separately and give evidence of the materials present and their amounts. Mixtures of poly(propylene) and poly(ethylene) have been analysed by DSC [56] and the components in recycled polymer waste have been detected by DTA [57].

HEAT CAPACITY MEASUREMENTS

The amount of heat needed to raise the temperature of the sample by 1 K is its heat capacity, $C_{p,S}$, in joules per Kelvin and:

$$C_{p,S} = (\partial q_S / \partial T)_p$$

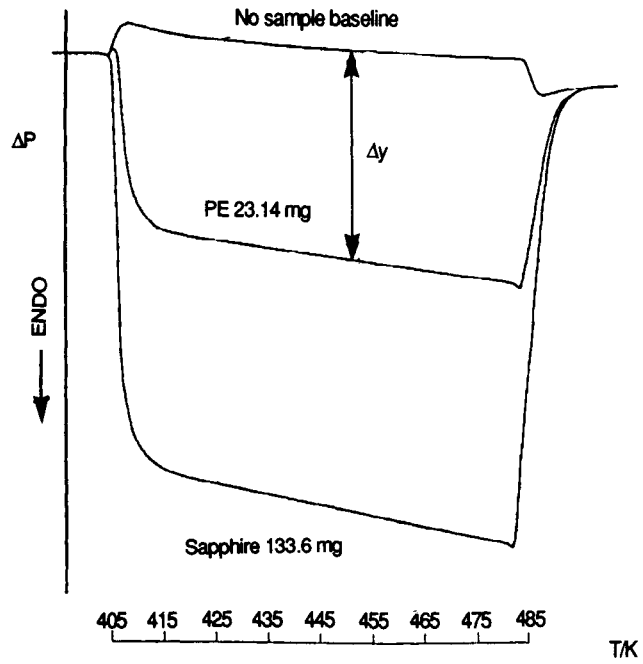

Figure 3.26 DSC curves for heat capacity measurement on molten polyethylene (PE).

On a DSC instrument, the calibrated y axis represents the differential rate of supply of heat energy, or ΔPower or $(\mathrm{d}\Delta q/\mathrm{d}t)$. Since we are heating at a constant rate, $(\mathrm{d}T/\mathrm{d}t)$, the product of the y axis deflection Δy from the baseline with no sample, divided by the heating rate, should give the difference in heat capacity due to the sample.

$$C_{p,S} = K \cdot \Delta y \,/\, (\mathrm{d}T/\mathrm{d}t)$$

where K is a calorimetric sensitivity, found by calibration.

Generally the calibration is done with sapphire, pure, crystalline Al_2O_3, whose heat capacity is well known.

Note: The higher the heating rate, $(\mathrm{d}T/\mathrm{d}t)$, the greater the deflection obtained!

The 'no sample' baseline can be used to correct for the effects of the reference side.

Exercise *Given that the heat capacity of sapphire at 445 K is 0.997 J/(K g) and the data in Figure 3.27, calculate C_p for PE. The heating rate is 20 °C/min.*

C_p (sapphire) $= 0.997 \times 133.6 \times 10^{-3} = 0.1332$ J/K
Δy (sapphire) $= 75.0$ mm
C_p (sapphire) $= (K \times 75)/\ 20 = 0.1332$

Thus

$$K = 3.552 \times 10^{-2} \text{ J/(min mm)}$$

For the polyethylene

$$\Delta y = 34 \text{ mm}$$

so

$$C_p(\text{PE}) = (3.552 \times 10^{-2} \times 34)/ 20 = 0.0604 \text{ J/K}$$

and since the mass of polyethylene is 23.14 mg,

$$C_p(\text{PE}) = 2.609 \text{ J/(K g)}.$$

This agrees quite well with literature values [59]. Wunderlich has published considerable data relating to the heat capacity of polymers [60,61].

The heat capacity is a most important quantity to know for many polymers, insulators and building materials [62].

GLASS TRANSITION TEMPERATURES

Below a certain temperature, known as the glass transition temperature T_g, the polymer segments do not have enough energy to rearrange or to rotate themselves. Such a material is brittle and a *glass*. As the sample is heated, there is a small increase in volume and energy, until at T_g the chains become more mobile and the polymer more plastic or rubbery. Further heating, as shown in Figure 3.27, allows the polymer to crystallise and then melt. Cooling from the melt directly may cause some of the polymer to crystallise at T_m. These changes are shown diagrammatically in Figure 3.27 and the T_g for various polymers is shown in Figure 3.28.

At the glass transition temperature, the heat capacity of the sample increases, since the chains acquire further freedom of movement. Therefore we observe a step and an increase ΔC_p, and also a change in the expansion.

It must be clearly recognised that the T_g is a *time-dependent phenomenon*! A polymer may slowly distort at a low temperature, but may behave in a brittle fashion when bent rapidly. While the T_g bears a marked resemblance to true second-order thermodynamic transitions [64] which always occur over a fixed, equilibrium temperature range, the value obtained for T_g depends greatly on the heating and cooling rates used in the DSC run.

If the heating rate is very low, say 0.1 K/min, the T_g may be low, say 80 °C, and this value is obtained again if the sample is cooled at the same rate. However, if the same sample is heated and cooled at 20 K/min the T_g

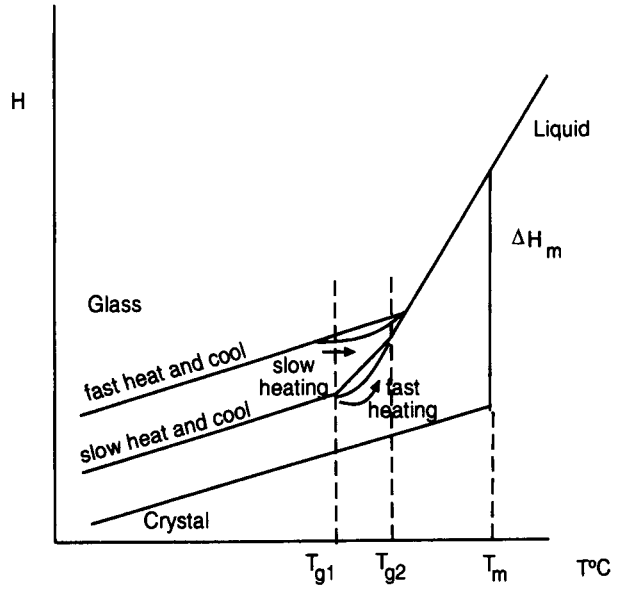

Figure 3.27 Schematic energy changes for material forming a glass.

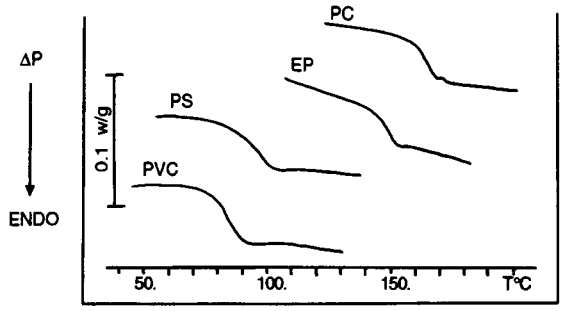

Figure 3.28 DSC curves showing the glass transitions for several polymers. All samples about 20 mg as received, run at 10 K/min in flowing nitrogen. PVC = poly(vinyl chloride); PS = polystyrene; EP = cured epoxy resin; PC = polycarbonate [63].

rises to 85 °C or higher! What happens if the heating and cooling rates are *not* the same? The sample that has been cooled slowly (say 0.1 K/min) goes through its T_g at 80 °C. If it is then heated at 20 K/min it does not transform till 85 °C. This means that the sample must absorb more energy to reach the enthalpy of the rubbery state. This results in an *endotherm*, superimposed on the glass transition step. This is shown in Figure 3.29.

The heating and cooling rates must therefore be stated, and the T_g also depends on molecular weight, degree of cure and amount of plasticiser present [65,66].

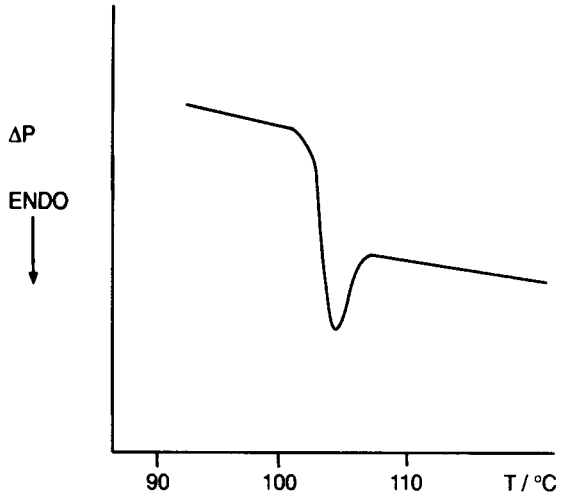

Figure 3.29 DSC curve for polystyrene cooled at 0.2 K/min and then heated at 5 K/min. (After Wunderlich [65].)

PURITY MEASUREMENTS

The determination of the absolute purity of a material is of highest importance for the characterisation of pharmaceuticals, insecticides, pure organics and metals. The theory [67] assumes that there are two effective components that give the eutectic phase diagram of Figure 3.30.

Thermodynamics shows that for a slightly impure A, containing x_B mol% of impurity B, the van't Hoff equation applies and the freezing point is lowered from that $T_{0,A}$ of pure A to T_m [68]. ΔT is given by:

$$\Delta T=(T_{0,A} - T_m) = (RT^2_{0,A}/\Delta H_{fus,A})\cdot x_B$$

When the mole fraction of impurity is small, ΔT must also be small, but the DSC peaks are found to be much broader for impure samples than for pure. The reason for this involves the *gradual* melting of the impure sample.

Consider the section of the eutectic diagram close to the pure A axis. The lines may be regarded as approximately straight, and we may construct similar triangles as shown. Since melting starts at the eutectic, the tie line PQR may be divided so that the ratio of the liquid solid is

Fraction liquid/fraction solid = PQ/QR
or Fraction melted, F = PQ/PR

From consideration of similar triangles, this may be put equal to the ratio of temperature intervals on the y axis.

$$F = (T_{0,A} - T)/(T_{0,A} - T_m) = (T_{0,A} - T)/\Delta T$$

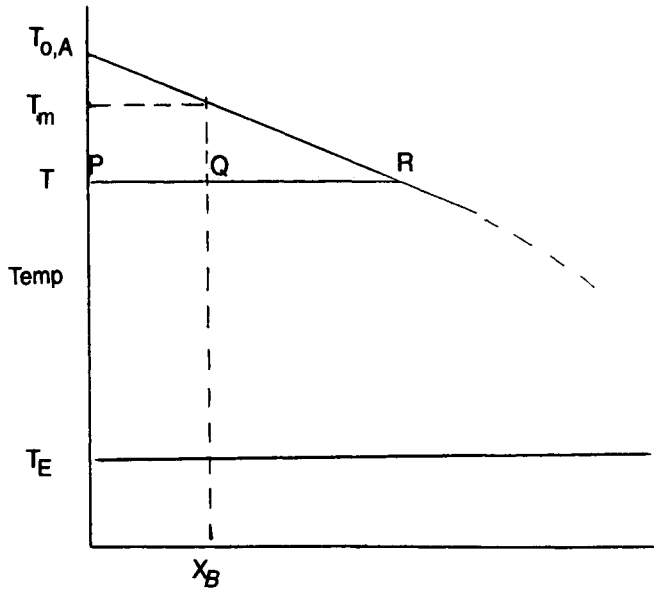

Figure 3.30 Section of eutectic diagram close to pure A.

Substitution into the van't Hoff equation gives:

$$(T_{0,A} - T) = (1/F)\cdot(RT_{0,A}^2/\Delta H_{fus,A})\cdot x_B$$

or, rearranging,

$$T = T_{0,A} - (1/F)\cdot(RT_{0,A}^2/\Delta H_{fus,A})\cdot x_B$$

This predicts that a plot of temperature versus $(1/F)$ should be a straight line of slope dependent on x_B, $T_{0,A}$, and $\Delta H_{fus,A}$. The temperature T may be corrected for thermal lag, measured using the peak for the melting of pure indium (Figure 3.11) or by the built-in software of the instrument [69].

From a DSC trace (Figure 3.31) obtained at the slowest heating rate possible, we may measure $\Delta H_{fus,A}$ and $T_{0,A}$ approximately, and the fraction melted at T °C from the ratio of the area a up to T, divided by the total peak area A.

$$F = a/A$$

Ideally this gives a good straight line. However, there are several factors which combine to produce a curve:

- neglect of any pre-melting before the peak measured
- non-equilibrium conditions, due to dynamic heating
- solid-solution formation.

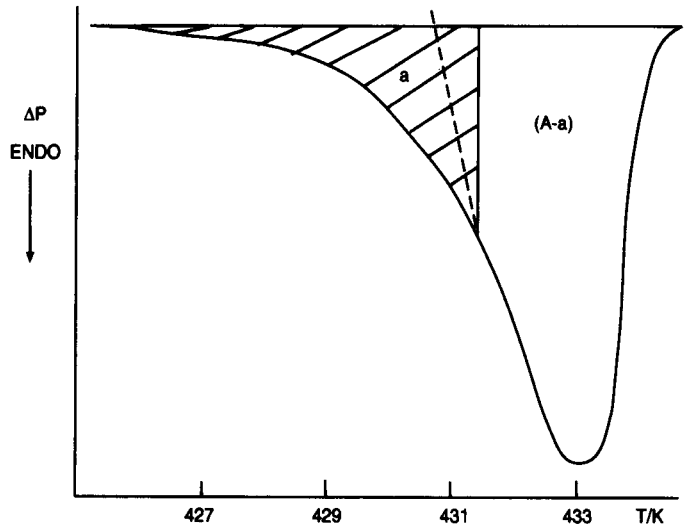

Figure 3.31 DSC trace of an impure material showing partial area measurement and temperature correction.

A correction for these factors that has been shown to be effective involves the use of an add-on correction da

$$F' = (a+\mathrm{d}a)/(A+\mathrm{d}a)$$

and

$$\Delta H_{\mathrm{fus,A}} = K\cdot(A+\mathrm{d}a)$$

This can be related to the modified van't Hoff equation for solid solutions [70]

$$\Delta T' = (1-k)\cdot(RT^2_{0,\mathrm{A}}/\Delta H_{\mathrm{fus,A}})\cdot x_{\mathrm{B}}$$

where k is the distribution coefficient for the solid solution.

In a different approach to eliminating the non-equilibrium effects, the use of discrete steps in heating has been suggested. If a step of less than 1 K is used and the system is then allowed to equilibrate, the trace produced shows peaks of equal area until melting commences. The peaks then increase until melting is complete. The sum of the peak areas, corrected for the heat capacity effect, gives values for a and A.

Plato and Glasgow [71] used the method to measure the purity of many compounds and it forms the basis of the ASTM method E928–85. Comparing the DSC and NMR methods of determining purity, Garn *et al.* [72] have shown that solid-solution formation plays a large role in determining the melting behaviour.

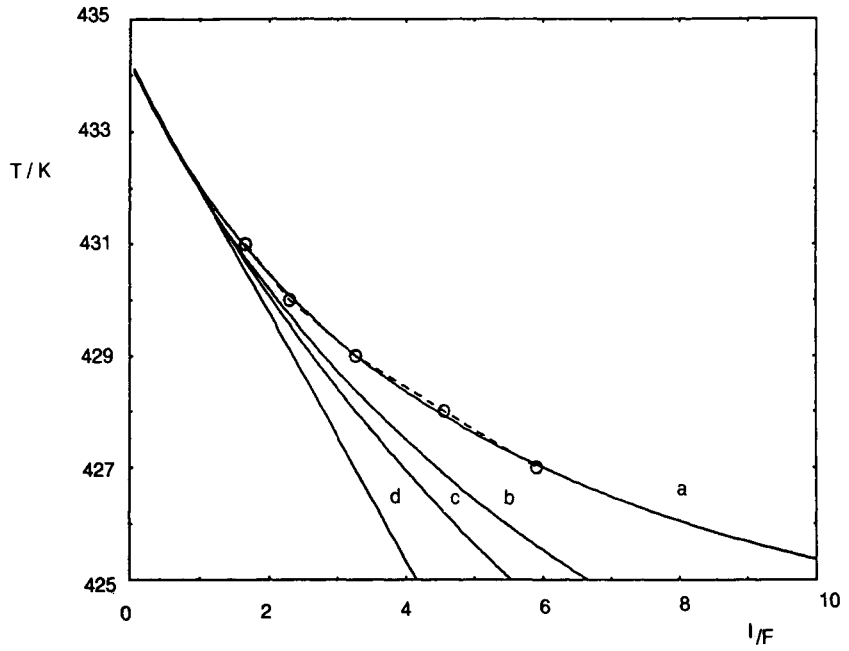

Figure 3.32 Plots of T/K versus $1/F$ and corrected $1/F$: (a) uncorrected; (b) 5% correction; (c) 10% correction; (d) 19% correction.

Example *A 3 mg sample of an insecticide (RMM = 365) was melted on a DSC at 1 K/min and gave the following results*:

T/K	a/cm^2	F	Total area, A = 10.5 cm^2
427	1.78	0.170	K = 10.0 mJ/cm^2
428	2.31	0.220	
429	3.21	0.306	
430	4.58	0.436	
431	6.33	0.603	

Calculate $T_{0,A}$, $\Delta H_{fus,A}$ and x_B.

A straightforward plot of T against $1/F$ gives a curve, intersecting the T axis at about 434 K (Figure 3.32(a))

We may treat the data in three ways:

1. Continue adding small amounts to a and A until a straight line is obtained;
2. Plot $(1/(T_{0,A} - T))$ versus F. The slope should give k.
3. Do a regression analysis of the curve.

1. Successive additions of 0.5 cm^2 to the area give a best line when the correction is about 2.0 cm^2, and this gives a a corrected total area of 12.5 cm^2, so that the corrected ΔH is about 15.2 kJ/mol and the slope of -2.2 gives an x_B value of 2.1 mol% (97.9% pure A). This is shown in Figure 3.32.

2. If we rearrange the equations above, we find that a plot of $1/(T_{0,A} - T)$ versus F should be a straight line of slope $(\Delta H/RT_{0,A}^2)/x_B$ and intercept related to the correction, k. If we assume that $T_{0,A} = 434$ K and make this plot, we get a value of x_B of 0.028, or a purity of 97.2%.

3. Although this requires considerable time, or computation, it is probably the best way ([19], Ch. 14). Regression analysis gives a correction of 0.163 and a purity of 97.9%.

3.9.2 *Chemical reactions*

KINETICS OF REACTION FROM DSC TRACES

Chemical reactions, and some physical changes such as cold crystallisation, occur at a temperature-dependent rate and involve an energy change, ΔH. We have seen how this may be related theoretically to the peak area and we may make assumptions about the relationship between the rate of supply of heat, which gives the ΔP signal, and the rate of reaction. For the heat capacity part of the change, which does *not* depend on the rate of reaction but on the material present at a particular time, we can draw in a proposed baseline. We must also use small samples and control the instrument carefully so that the temperature gradients within the sample are very small.

Provided we may make these assumptions, the peak that we obtain, either for a scanning or for an isothermal run, may be divided into fractions representing the fraction of reaction α which has occurred.

The kinetic equations have been described in Chapter 2, and may be very complex. The analysis of data is best done for a simple single-stage process. If we are dealing with a multi-stage reaction, for example the decomposition of a polymer, it is very difficult to assign kinetic parameters to the stages of reaction. Additional information is needed for the separate values of ΔH for each stage. The separate rates might be obtained by combining DSC with other analyses of products, for example by infrared spectrometry or evolved gas analysis.

Barrett [73] applied this method to the decomposition of free-radical initiators like azobisisobutyronitrile (AIBN). The DSC of AIBN in dibutyl phthalate at heating rates between 4 and 32 K/min gave kinetic data corresponding well to first order kinetics and an activation energy of about 125 kJ/mol in agreement with UV experiments.

Crystallisation rates of polymers have been measured [74, 75] using the partial area to determine the percentage crystallized. The results often fit an Avrami equation:

$$[-\ln(1-\alpha)]^{1/n} = kt$$

where α is the fraction of the final crystallinity developed at time t, and n

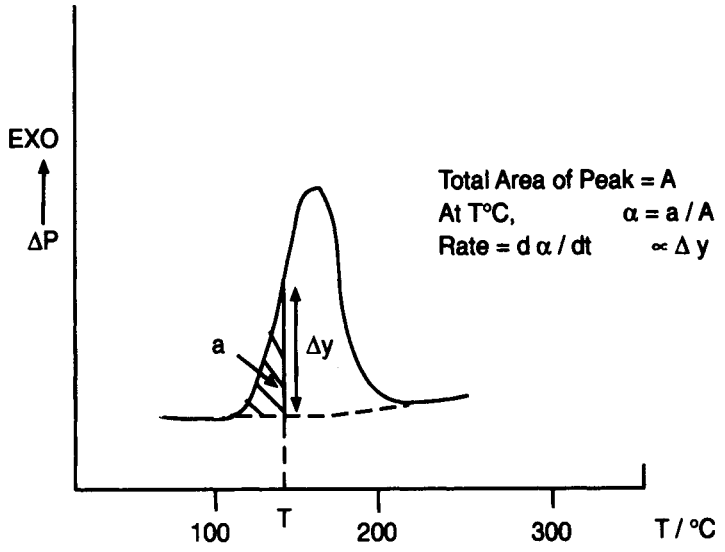

Figure 3.33 DSC curve for exothermic reaction showing measurement of partial and total areas.

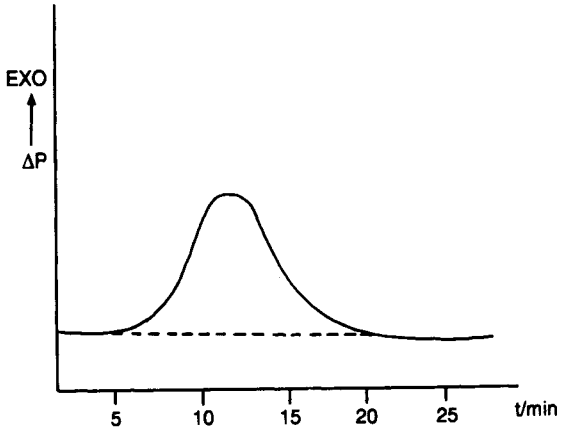

Figure 3.34 Isothermal DSC curves for polymer crystallisation.

depends on the mechanism of crystal growth, e.g. $n = 3$ for spherical growth.

The assessment of thermal hazards by analysing kinetic data is a standard ASTM method E698-79 [76]. The method recommended by this committee is that of Ozawa [77], where samples are run at several different heating rates, β, the temperature corresponding to the peak maximum T_{max} is noted. Ozawa showed that if ln(β) is plotted versus $1/T_{max}$ a straight

line of slope approximately E/R is obtained, and the values may be refined by using a correction factor.

3.9.3 *Inorganic compounds and complexes*

The dehydration, decomposition and other reactions that take place with inorganic chemicals and minerals were among the first reactions studied by DTA. We may obtain vital information about the endothermic or exothermic nature of the reactions, which may be compared with data from thermodynamic tables. We can detect melting and other phase changes, and the DTA (or DSC) trace itself is an effective 'fingerprint' of the thermal behaviour of the compound *under those particular conditions!*

CALCIUM OXALATE MONOHYDRATE ($CaC_2O_4 \cdot H_2O$)

Figure 3.35 shows the DTA curves of calcium oxalate monohydrate run under flowing air and under flowing nitrogen. The endothermic peak around 200 °C is due to the loss of the hydrate water, and is similar in both gases. In nitrogen, the peak around 400 °C is also endothermic, and corresponds to the breakdown of the oxalate with loss of carbon monoxide. When the atmosphere is oxidising, however, the CO is oxidised as soon as it is formed, and the peak becomes exothermic. The endothermic peak at 800 °C is due to the decomposition of the calcium carbonate, and is only slightly affected by the change of gas.

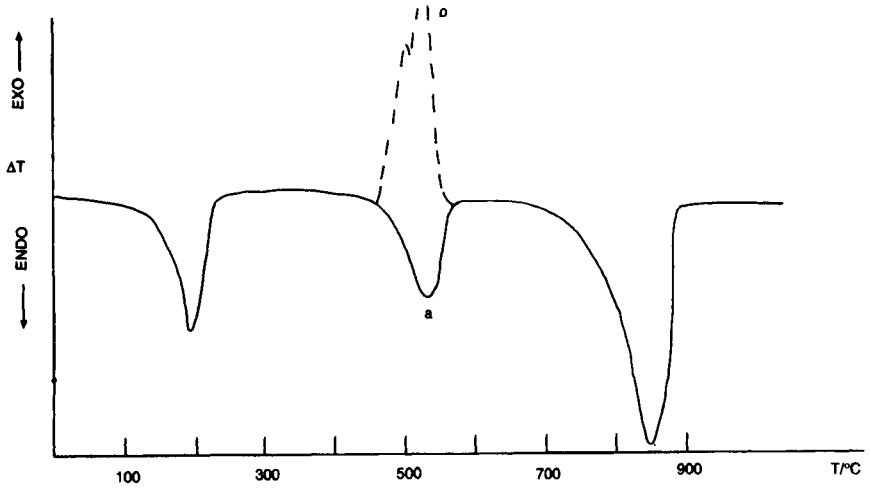

Figure 3.35 DTA curves for calcium oxalate monohydrate: (a) in nitrogen; (b) in air. Sample: 10 mg of powder, heated at 10 K/min.

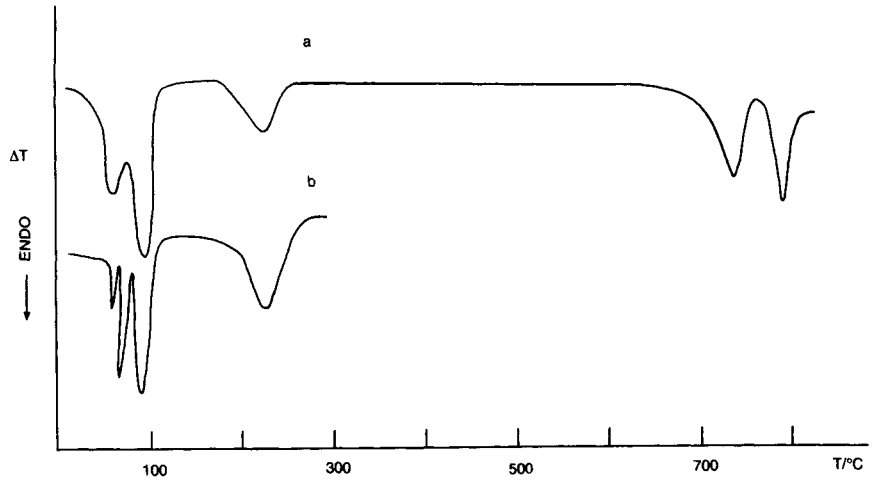

Figure 3.36 DTA curves for copper sulphate pentahydrate: (a) unsealed pan; (b) sealed pan with pinhole. Sample: 6 mg crystalline powder, 10 K/min, flowing air.

The effects on the DTA curve of changes in heating rate, sample mass and particle size, atmosphere and gas flow rate have all been thoroughly investigated for this system [78].

COPPER SULPHATE PENTAHYDRATE ($CuSO_4 \cdot 5H_2O$)

The dehydrations and decomposition of copper sulphate produce a series of endothermic peaks on the DTA or DSC trace (Figure 3.36).

The initial loss of water may produce traces that seem different, especially if different sample pans are used. A very open, flat pan will give two broad, overlapping peaks of roughly equal area around 120 °C. If the loss of water is restricted – for example, by using a lidded pan with a small pinhole only – then the water may be retained and boil off separately, giving a triple peak. At higher temperature, the final molecule of water is lost.

Calorimetric measurements on the dehydration peaks gives ΔH values of approximately:

$$CuSO_4 \cdot 5H_2O = CuSO_4 \cdot 3H_2O + 2H_2O \quad \Delta H\ (373\ K) = 100\ kJ/mol$$
$$CuSO_4 \cdot 3H_2O = CuSO_4 \cdot H_2O + 2H_2O \quad \Delta H\ (400\ K) = 104\ kJ/mol$$
$$CuSO_4 \cdot H_2O = CuSO_4 + H_2O \quad \Delta H\ (510\ K) = 72\ kJ/mol$$

The sample decomposes to the oxide at higher temperatures:

$$CuSO_4 = CuO + SO_2 + \tfrac{1}{2}O_2$$

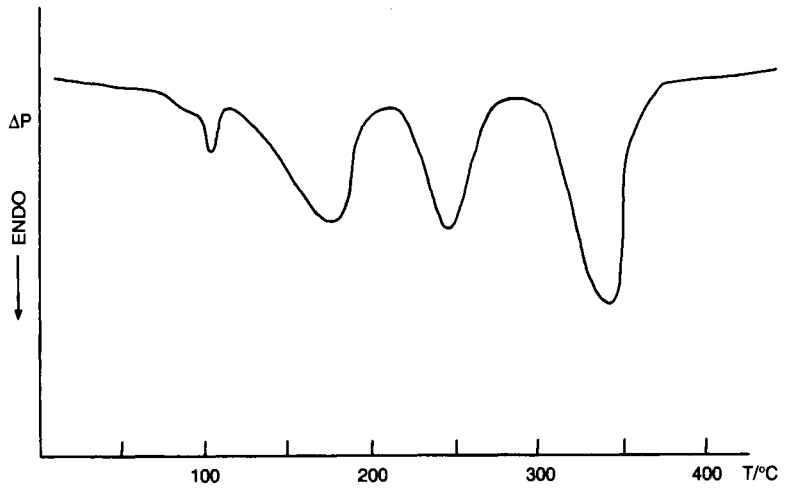

Figure 3.37 DSC curve for cobalt pyridinium chloride (3.4 mg, 8 K/min, flowing nitrogen) [81].

METAL COMPLEXES

Very many complex compounds have been investigated by DSC [79, 80, 81 and general texts] and the effects of the metal and the ligand on the reactions and the reaction enthalpies measured. The important factors are the loss of the ligand, phase changes and decompositions of the sample and of the products. For these complicated reactions, it is advantageous to use *simultaneous techniques* which will be discussed in Chapter 5. One example of the calorimetric use of DSC is cobalt pyridinium chloride, $Co(C_5H_5N)_2 \cdot Cl_2$ [81], which gives four transitions up to 500 °C. At about 120 °C, a small, sharp endothermic peak with ΔH = 12.6 kJ/mol is obtained, but this corresponds to no mass loss in the TG experiment. Three subsequent peaks at 180, 280 and 350 °C, show progressive losses on the thermobalance, corresponding to loss of 1, 1/3, and 2/3 pyridine molecules respectively. The total ΔH for these reactions is about 120 kJ/mol(Fig. 3.37).

HIGH ALUMINA CEMENTS [82–85]

Ordinary Portland cement (OPC) is made by heating clays, which are aluminosilicates, with calcium carbonate, and consists chiefly of mixed calcium silicates. During their use, the cement is mixed with water which hydrates the silicates and produces a good cementing material, which very slowly develops its final strength over many months. The DTA curve of an OPC is given in Figure 3.38, which shows the dehydration of the material and also the peak due to the quartz transition at 573 °C.

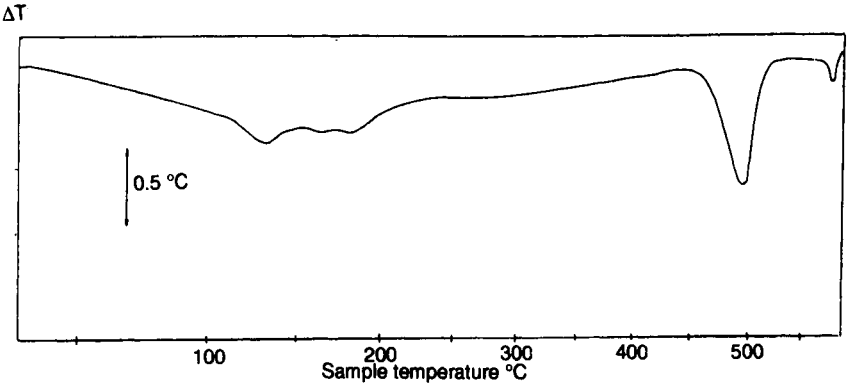

Figure 3.38 DTA curve for a Portland cement concrete sample (50 mg, 20 K/min, nitrogen).

High alumina cement (HAC) is made from bauxite and limestone, and is mostly a mixture of calcium aluminates. These react with water and gain strength more rapidly than OPC, and so they speed up the building process. Unfortunately, under certain conditions, beams constructed of HAC concrete collapsed catastrophically. A programme of testing was undertaken at once in which DTA played a most significant part.

The material which is first produced in the hardening process is the decahydrate

$$CaO{\cdot}Al_2O_3{\cdot}10H_2O \quad \text{abbreviated to } CAH_{10}$$

This is not the most stable hydrate, and may gradually undergo a 'conversion' reaction to more stable compounds, such as the hexahydrate and hydrated alumina or gibbsite.

$$3CaO{\cdot}Al_2O_3{\cdot}6H_2O \text{ (or } C_3AH_6) \quad \text{and} \quad Al_2O_3{\cdot}3H_2O \text{ (or } AH_3)$$
$$3(CaO{\cdot}Al_2O_3{\cdot}10H_2O) = 3CaO{\cdot}Al_2O_3{\cdot}6H_2O + Al_2O_3{\cdot}3H_2O + 18H_2O$$

This conversion weakens the structure, because the products of reaction are more dense and the reacted structure more porous, particularly if conversion has taken place rapidly.

The decahydrate, the hexahydrate and gibbsite, plus several other hydrates, all lose water over specific temperature ranges, as indicated in Figure 3.39. All the dehydrations are endothermic, and the sample will show these dehydrations clearly by DTA. It is also helpful to run to 600 °C to show the silica peak, but also to show the dehydration peak of $Ca(OH)_2$ at 500 °C which is characteristic of OPC.

The method of sampling is important, since high-speed drilling might heat the sample above the dehydration temperatures. Plaster should be removed, since the dehydration peaks of gypsum and plaster of Paris occur in the region of interest for HAC. The slowly drilled out samples should be

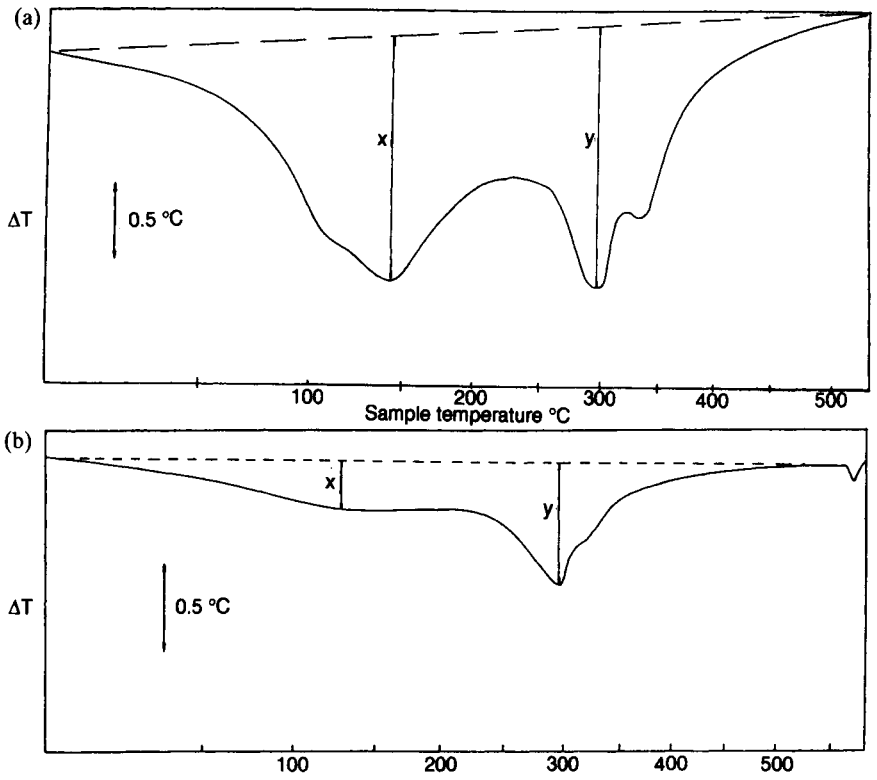

Figure 3.39 DTA curves for HAC standards having conversions of (a) 50% and (b) 70% [83].

sieved to remove large particles, and metallic particles from the drilling should be removed with a magnet.

Samples of 10–100 mg are run in flowing nitrogen at heating rates between 10 and 30 K/min, and calibration standards run under the same conditions. The 'degree of conversion', D_c, is calculated from the *height* of the peaks measured, as shown on Figure 3.39.

$$D_c = \frac{100 \cdot \text{Amount of } AH_3}{(\text{Amount of } AH_3 + \text{amount of } CAH_{10})}$$

$$\text{or } D_c = \frac{100 \cdot a \cdot (\text{Height of } AH_3 \text{ peak})}{(a \cdot \text{Height of } AH_3 \text{ peak} + b \cdot \text{Height of } CAH_{10} \text{ peak})}$$

$$\text{or } D_c = \frac{100 \cdot (\text{Height of } AH_3 \text{ peak})}{(\text{Height of } AH_3 \text{ peak} + K \cdot \text{Height of } CAH_{10} \text{ peak})}$$

where a and b are calibration constants and $K = b/a$.

Examples of the calculation of degree of conversion should not be quoted to better than ± 5%

Calculation The calibration constant K was determined by running standard samples with 50 and 70% conversion. For the 50%, the AH_3 peak height was 3.5 cm and the CAH_{10} peak height 3.7 cm. Therefore:

$$50\% = 100 \times 3.5/(3.5 + K \times 3.7)$$

Thus $K = 0.95$.

For an unknown HAC sample, the AH_3 peak was 4.4 cm high, and the CAH_{10} peak 2.6 cm high. Therefore:

$$D_c = 100 \times 4.4/(4.4 + 0.95 \times 2.6)$$
$$D_c = 64 \pm 5\% \text{ conversion.}$$

CLAYS AND OTHER MINERALS

The literature describing applications of DTA on minerals is very large [82, 86–88], and only a few typical examples will be described here.

We have already seen from the HAC experiments that minerals give characteristic DTA traces. Single component minerals, such as quartz, show their phase transitions. Hydrated and hydroxyl minerals show dehydration peaks, and carbonate minerals lose carbon dioxide. Typical traces are shown in Figure 3.40.

Kaolinite, or china clay, is an important industrial mineral. The DTA trace of Figure 3.41 shows a small, broad endothermic peak at about 100 °C and a much larger endotherm at 550 °C. A sharp *exotherm* appears at about 1000 °C. These have been interpreted as loss of moisture at 100 °C, dehydroxylation by 700 °C and the reaction to form a new crystalline material, chiefly mullite ($3Al_2O_3 \cdot 2SiO_2$).

Borate minerals have very complex structures and cannot always be characterised by elemental analysis. For a series of minerals of general formula $M_2B_6O_{11} \cdot xH_2O$, some containing discrete anions (Figure 3.42(a)) lose most of their water below 250 °C while others which have linked chains do not decompose until much higher temperatures (Figure 3.42(b)). Mixtures of these two types may be analysed semi-quantitatively by thermal methods [91].

3.9.4 *Synthesis of compounds at high temperatures*

The high-temperature reactions of inorganic compounds produce many new materials, some of which are of special interest to the electronics industry.

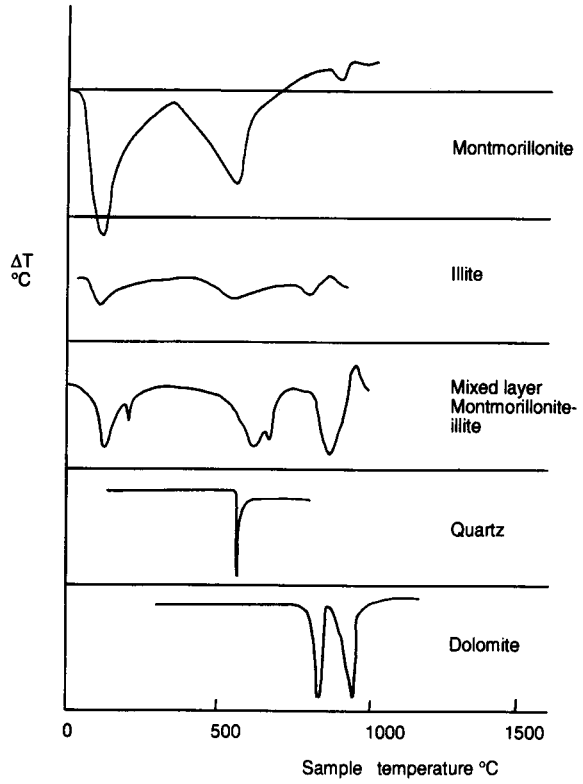

Figure 3.40 DTA curves of some common minerals [89].

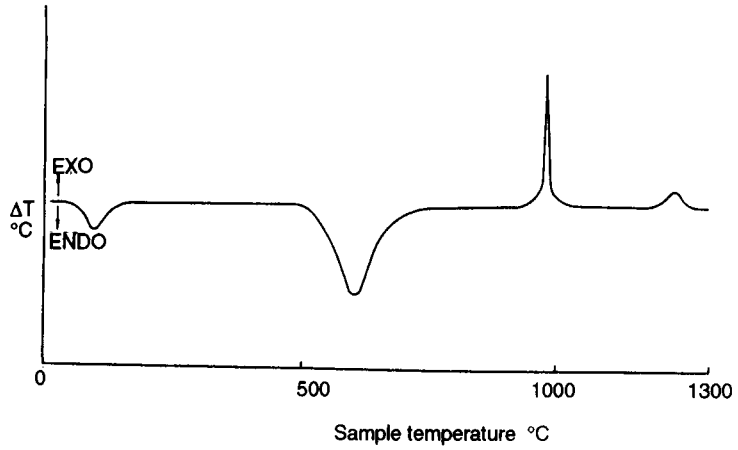

Figure 3.41 DTA curve of kaolinite [89].

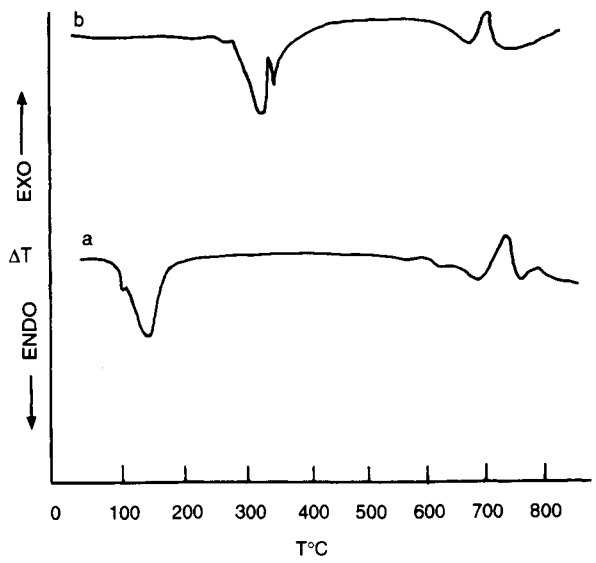

Figure 3.42 DTA curves for triborate minerals: (a) Inyoite; (b) Colemanite. Samples of about 20 mg, 10 K/min, static air [91].

Heating together barium carbonate and iron(III) oxide in the molar ratio 1:6 gives the DTA shown in Figure 3.43.

When heated alone, barium carbonate shows sharp crystal phase transitions at 810 and 970 °C while iron oxide shows a transition at 675 °C. Together, the mixture still shows the transition at 675 °C but now a large, broad endotherm appears with a maximum at 870 °C. X-ray analysis of the final product shows it to be barium hexaferrite, $BaFe_{12}O_{19}$. This material is a valuable magnetic solid used as cores for inductive components.

Similar experiments can be conducted to produce a phosphor from barium hydrogen phosphate $BaHPO_4$ heated with about 10% TiO_2 to 1070 °C, when a material is produced which phosphoresces brightly in the visible when illuminated with UV light [93].

3.9.5 *Pyrotechnics*

The reactions involved in pyrotechnics may be studied by DTA or DSC since the small samples and programming allow good control of the system. The reactions of 'black powder' (powdered sulphur, potassium nitrate and charcoal) have been studied by DTA, TG and DSC [94]. The DTA in nitrogen shows the phase transitions of sulphur and of KNO_3, vaporisation of sulphur followed by the exothermic reaction between charcoal and potassium nitrate between 390 and 550 °C and the decomposition of unreacted potassium nitrate (Figure 3.44). In air, there are two exotherms

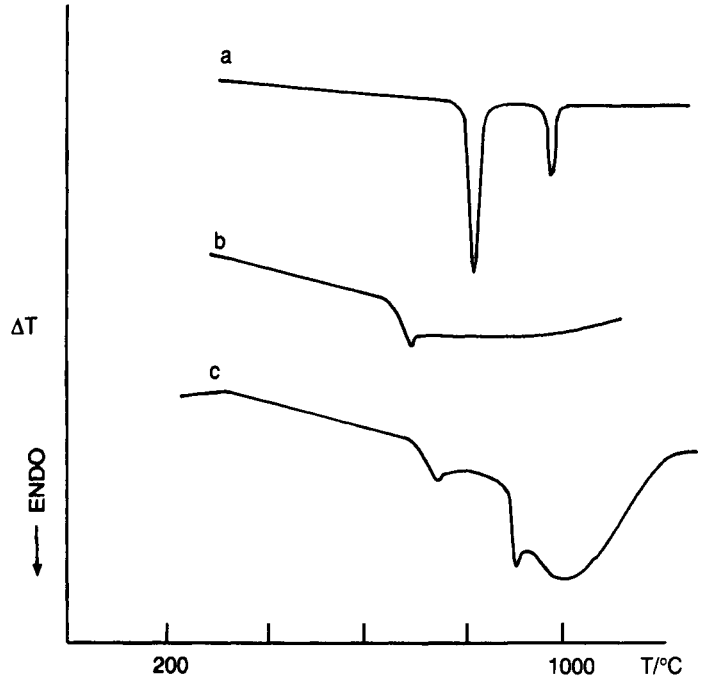

Figure 3.43 DTA curves for (a) $BaCO_3$, (b) α-Fe_2O_3, (c) mixture of $BaCO_3$:$6Fe_2O_3$.

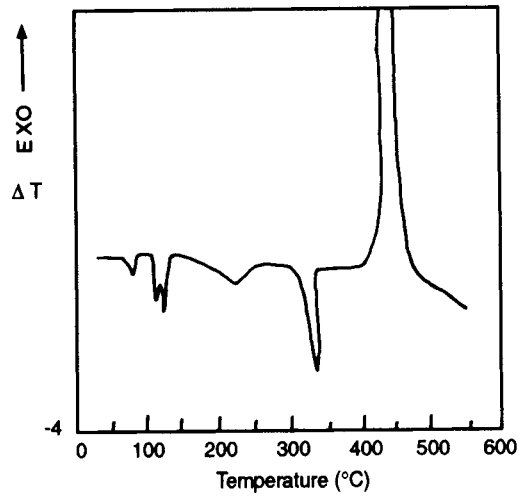

Figure 3.44 DTA of black powder in nitrogen at 20 K/min (After [94]).

due to the oxidation of sulphur at above 190 °C and then oxidation of charcoal. A review of applications of thermal analysis to pyrotechnic systems gives many other examples [95].

3.9.6 *Superconductors*

The discovery of the new materials whose superconducting properties extended to much higher temperatures than before, has given a great impetus to studies of high T_c superconducting ceramics. The synthesis of yttrium barium copper oxide materials has been reviewed by Ozawa [96], and Chen and Sharp report DTA studies on a high-temperature synthetic method [97].

The reaction between Y_2O_3, BaO_2 and Cu metal in the proportions 0.5:2:3 on heating in oxygen is exothermic, as shown in Figure 3.45. They showed that there is no reaction between Y_2O_3 and copper when they are heated alone, but that Y_2O_3 and BaO_2 reacted exothermically to produce Y_2BaO_4. Copper and barium peroxide reacted very vigorously to produce $BaCuO_2$, and the ternary mixture gave a DTA which resembled a combination of these two reactions, producing $YBa_2Cu_3O_y$ (y = 6–7) and Y_2BaCuO_5 detected by X-ray diffraction.

3.9.7 *Organic compounds*

The reactions of organic materials and of polymeric materials, both natural and synthetic, have been widely studied by DTA and DSC. The effects of the atmosphere are very important here, since oxidative degradation may occur by a very different mechanism to non-oxidative changes.

OXIDATIVE DEGRADATION

Polymers and also oils degrade when heated in oxidising atmospheres. A standard test for this has been devised and may be used to compare the stabilities of polyolefins and of other oils and fats.

The sample may be heated in nitrogen to 200 °C and the atmosphere then changed to oxygen, with the temperature held constant at 200 °C. The time for the onset of the exothermic oxidation is then noted. Alternatively, the polymer may be heated in oxygen and the temperature at which the onset of oxidation occurs noted.

The same type of test may be applied to lubricants, and to edible oils and fats, and has been used to test the efficiency of anti-oxidants.

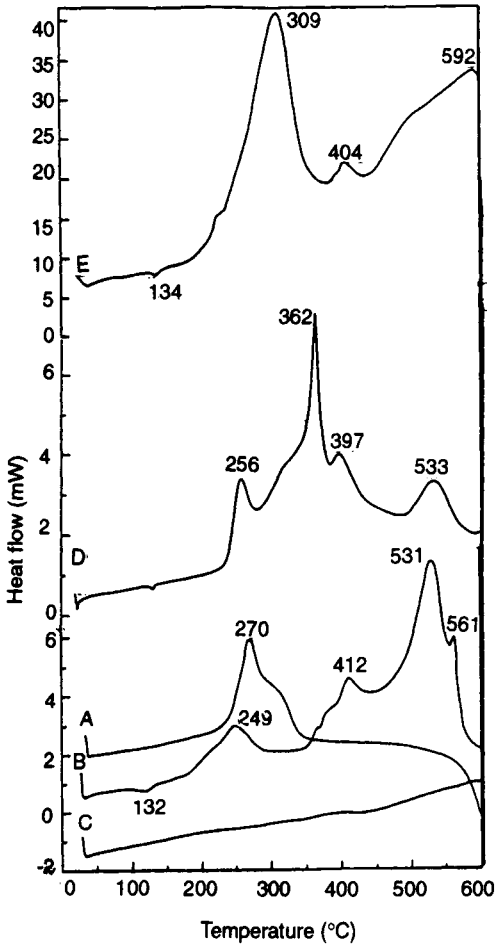

Figure 3.45 DSC curves for superconductor components: curves A to D 10 K/min in nitrogen; curve E 50 K/min in nitrogen [95].
A: $0.5Y_2O_3 + 2BaO_2$ B: $2BaO_2 + 3Cu$
C: $0.5Y_2O_3 + 3Cu$ D and E: $0.5Y_2O_3 + 2BaO_2 + 3Cu$

POLYMER CURE [100]

The reaction of small molecules to produce larger molecules with different properties and more stability is generally exothermic. The average ΔH of polymerisation of unsaturated molecules like styrene and vinyl chloride is about -100 kJ/mol. The reactions of thermosetting polymers, such as epoxy resins and polyesters cross-linked with styrene, are also exothermic and readily studied by DSC.

The reaction of the epoxy group with a curing agent, often an amine, is the initial stage in the reaction and is followed by a further reaction of the secondary amine with a further epoxy group.

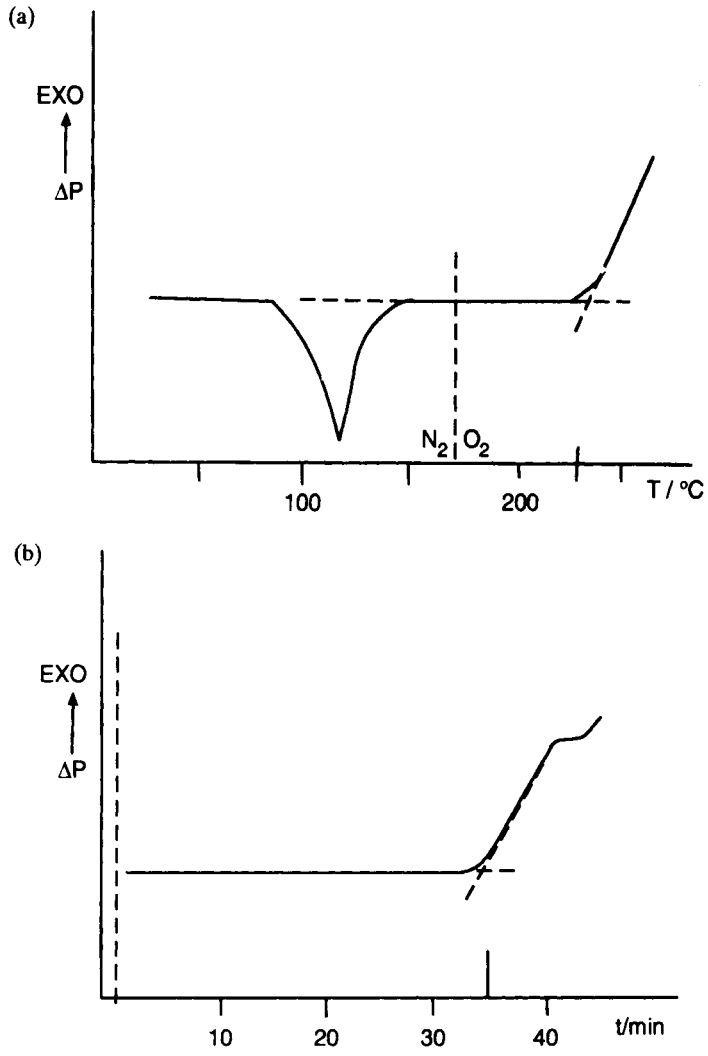

Figure 3.46 DSC curves for oxidation of polyethylene. The dashed line represents the changeover from nitrogen to oxygen. (a) Scanning DSC for PE film, 10 K/min; onset temperature of oxidation = 220 °C. (b) Isothermal DSC for PE film at 200 °C; onset time = 35 min.

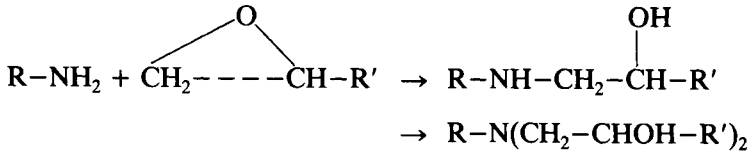

This reaction occurs even at low temperatures, but is rapid above 100 °C,

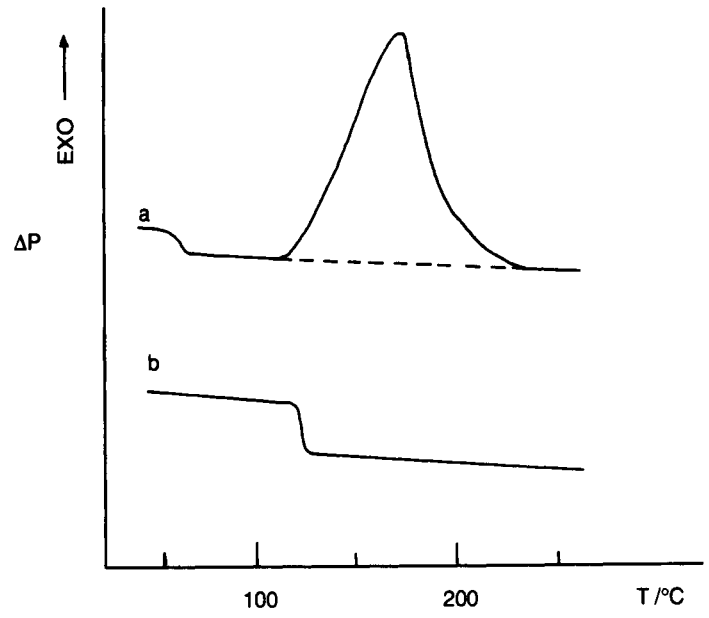

Figure 3.47 Schematic DSC for typical epoxy cure. Samples of 5 mg, 10 K/min, nitrogen. (a) Initial run of uncured sample; (b) re-run of fully cured material.

giving the DSC trace of Figure 3.47. The initial T_g of the starting material is followed by the large exotherm of the reaction. Re-running the cured material shows a new T_g at a much higher temperature. Post-curing will raise this T_g to even higher temperatures.

The kinetics of the reaction may be studied from scanning or an isothermal experiment.

PROTEIN DENATURATION

Proteins may be classified as fibrous, with long thread-like molecules, for example collagen, or globular, with compact 'spherical' shapes such as insulin. Both types have well-developed structures involving folds, coils or sheets and even a helix within a helix: a 'super-helix'. These structures are destroyed by heating or denaturation at extreme pH, and this reaction is endothermic.

Figure 3.48(a) shows the denaturation of collagen, a single material, while Figure 3.48(b) shows the complex behaviour of multi-component systems found in real animal muscle proteins. Note the large sample and slow heating rate used here [102].

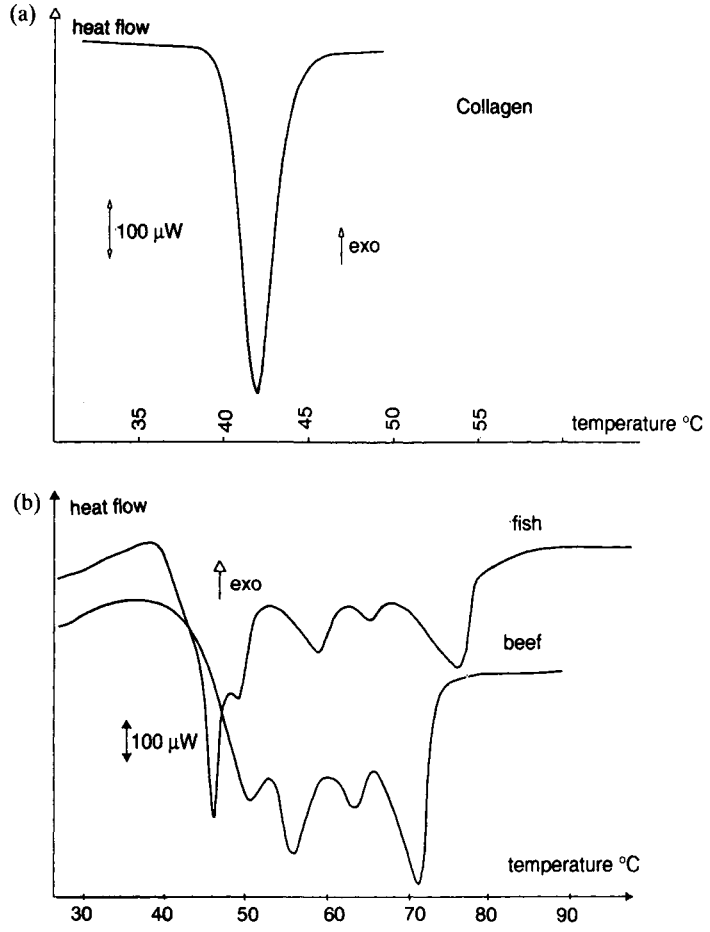

Figure 3.48 Micro-DSC curves for denaturation of proteins [102]. (a) 800 mg, 0.3% collagen solution, sealed vessel, 0.5 K/min; (b) 850 mg beef and fish muscle, sealed vessel, 0.2 K/min. (Courtesy SETARAM)

POLYMER DEGRADATION [20,103]

The complex reactions that occur when polymers degrade in inert or oxidative atmospheres have been discussed in Chapter 2. DTA and DSC studies will give further information on the stages and enthalpy changes involved.

The DTA curves for the oxidative decomposition of poly(vinyl chloride) (PVC) and of polypropylene (PP) are shown in Figures 3.49 and 3.50.

PVC powder shows a small glass transition around 80 °C and then a small endotherm near 300 °C, almost immediately followed by a very large exotherm peaking at around 550 °C. These later stages correspond to the

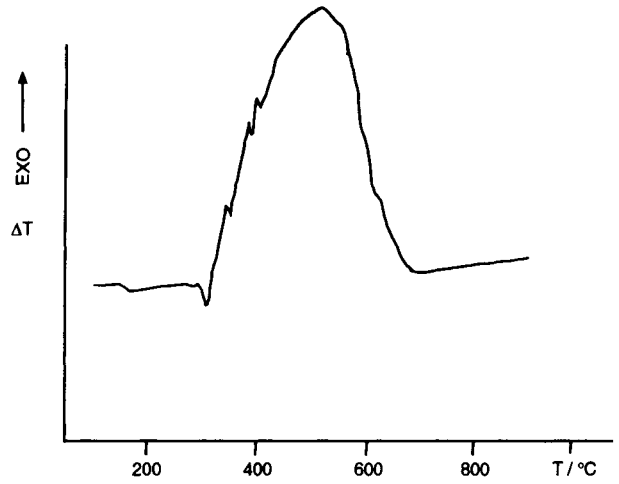

Figure 3.49 DTA curve for poly(vinyl chloride). Geon powder, 20 mg, 15 K/min, flowing air.

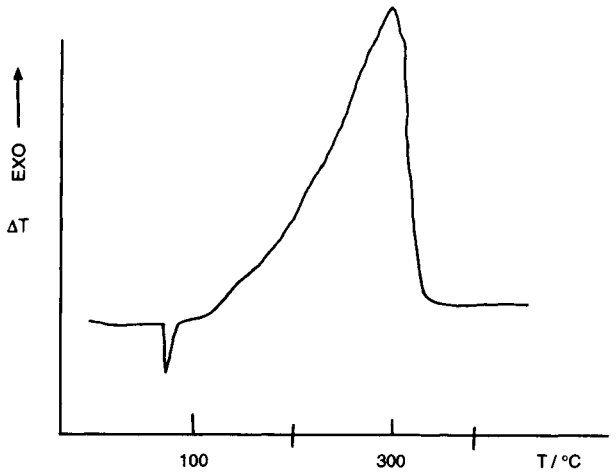

Figure 3.50 DTA curve for unstabilised polypropylene film, 20 mg, 15 K/min, flowing air.

degradation with loss of HCl and flammable volatiles, followed by oxidation of the char which is formed.

PP decomposes in a single stage and the products are then easily oxidised, so a single endothermic peak is obtained for the melt, followed by a large oxidation peak.

3.10 Specialist DSC systems

3.10.1 *Pressure DSC (PDSC)*

By placing the entire DSC or DTA cell in a pressure-tight enclosure, it is possible to work at pressures less than atmospheric, or more than atmospheric.

A simple modification of DSC and DTA equipment [104] allowed reasonably accurate determination of boiling points of organic liquids in the pressure range 20–760 mm Hg. Seyler [105] investigated the parameters affecting this type of measurement, especially the cell design and sample size. Recent work [106] using hermetically sealed pans with 50–100 μm laser-drilled holes gives vapour pressures within a few percent. Results for the vaporisation of water at pressures up to 3.5 MPa gave excellent agreement with literature data [107].

It should be noted that in *raising* the boiling point, or sublimation temperature, any vaporisation which interferes with melting is suppressed, and better melting point, purity and phase data will be obtained.

In predicting the oxidative stability of oils, polymers and foodstuffs, the use of higher pressures of oxygen decreases the volatility of the material (because the boiling point increases with pressure increase) and also increases the concentration of reactant gas. Shorter test times are then possible, and if any volatiles are lost at high temperatures, then lower test temperatures and higher oxygen pressures may be used. These advantages are discussed by Thomas [108]. Oxidation and ignition of oils under a high pressure of nitrogen (8 MPa) with flowing oxygen was used to compare new and used oil samples and anti-oxidants [107].

Reductions of organic compounds with hydrogen using metal catalysts has been studied with PDSC. With platinum or palladium metal catalysts on a silica substrate, the catalyst sample is heated to reaction temperature in helium under pressure, and then the gas switched to hydrogen. Chemisorption and catalytic reduction produce an exotherm on the DSC, which can be related to the hydrogen consumed. If the desired ratio of reactant to react with 2–3 mg of catalyst is put into the DSC cell, a similar procedure produces an exotherm for the reduction of the reactant, for example, *m*-dinitrobenzene using a 5% Pd/carbon catalyst, as shown in Figure 3.51 [109].

Phase diagrams and reactions for praseodymium oxides, reduction of metal oxides, formation of a metal hydride and oxidation of charcoal [107] all demonstrate the usefulness of a pressure DSC system.

3.10.2 *Photocalorimetric DSC*

Polymerisation may be initiated by ultraviolet light, and this is used in many disciplines such as electronics, coatings and dental work. DSC cells have been adapted to measure the polymerisation exotherm while the

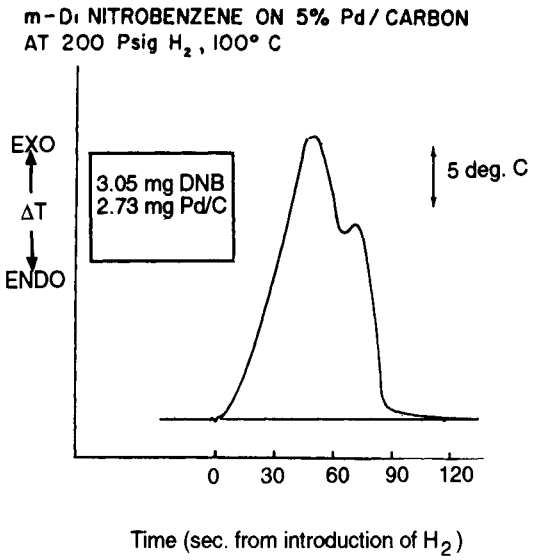

Figure 3.51 Isothermal PDSC trace for the reduction of *m*-dinitrobenzene [109].

sample is irradiated with UV [110]. The 'photocalorimeter' is made up of a DSC and an accessory which illuminates the sample cell with UV light of selected wavelength and intensity.

Tryson and Schultz [111] investigated the polymerisation of lauryl acrylate and of 1,6-hexanediol diacrylate using a DSC illuminated by a medium-pressure mercury lamp (λ_{max} = 365 nm) through a heat filter filled with de-ionised water and a manually operated shutter. The pans were modified so that a uniform sample thickness was maintained. A typical DSC cure curve is shown in Figure 3.52.

Manley and Scurr [112] used a DTA apparatus to study the UV curing of surface coatings of methyl methacrylate plus azobisisobutyronitrile (AIBN) and Hodd and Menon [113] investigated various initiators for the photopolymerisation of acrylates.

3.10.3 *Modulated DSC (MDSC™)*

The many changes that can be detected by DSC are both an advantage and a disadvantage! If the primary purpose is to detect a glass transition, and a second event such as a chemical reaction or crystallisation overlaps, how may we separate them?

In a conventional DSC, a constant, linear heating rate is applied. If the heating is 'modulated' by a small alternating amount of power supplied in addition to the normal programmed heating, the temperature should follow the profile shown in Figure 3.53 [114,115].

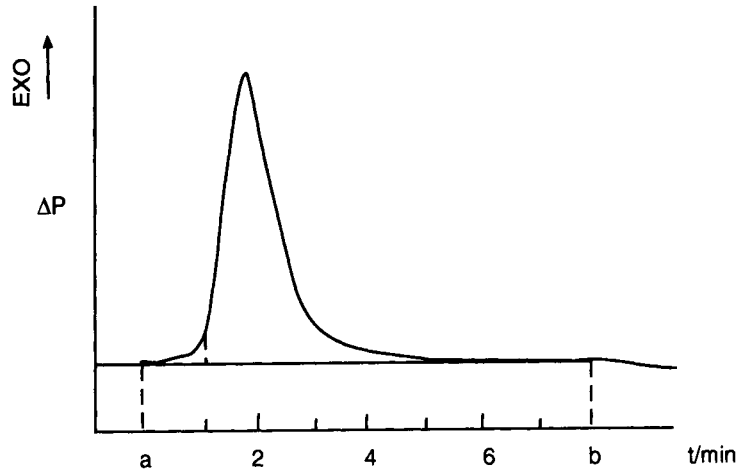

Figure 3.52 Schematic photo–DSC curve for a photo-initiated polymerisation. (a) UV on; (b) UV off.

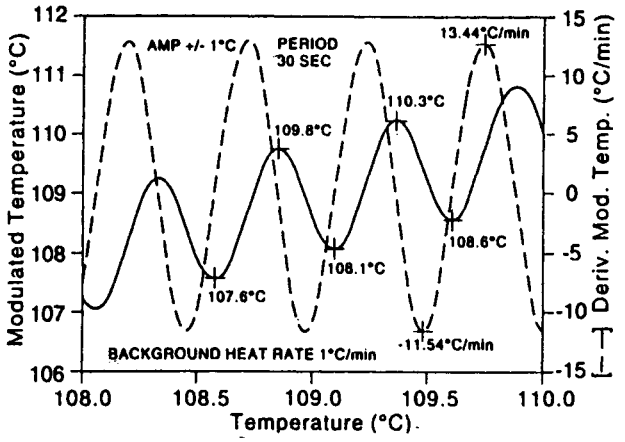

Figure 3.53 MDSC heating profile showing the overlaid ripple on the heating ramp.

When we have a heating programme such that

$$T = T_0 + \beta t + B \sin(\omega t)$$

where ω is the angular frequency ($= 2\pi f$), T_0 is the starting temperature and B is the amplitude of temperature excursion, then the heat flow is given by:

$$(dq/dt) = C_p[\beta + B{\cdot}\omega \cos(\omega t)] + \bar{f}(t,T) + C \sin(\omega t)$$

where C_p is the heat capacity, $\bar{f}(t,T)$ is the average underlying kinetic

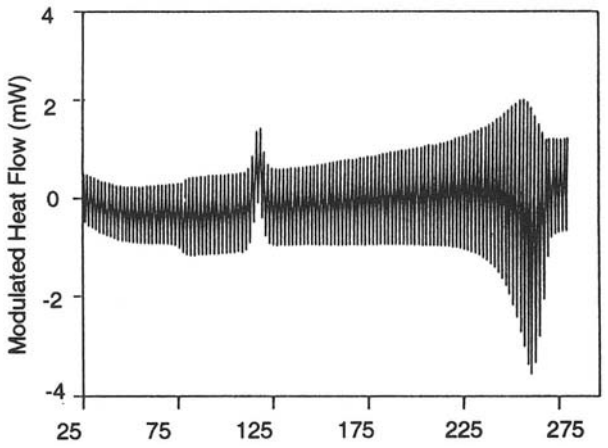

Figure 3.54 MDSC trace for quenched PET before deconvolution.

response and C is the amplitude of the kinetic response to the sine wave modulation.

The heat flow has a cyclic component which is made up of the sine and cosine terms, the amplitude of which is determined by a Fourier transform analysis. The underlying signal, which is equivalent to a conventional DSC, is calculated by an averaging process. The value of C is often low, so that the third term is negligible and the cyclic signal gives the heat capacity directly. By multiplying this by the heating rate the *reversing heat flow* is obtained. This is then subtracted from the underlying signal to obtain the *non-reversing heat flow*.

The main component of the reversing signal is the heat capacity, and thus the glass transition appears in this signal.

Other events which appear in the non-reversing signal are decomposition, curing of polymers, cold crystallisation, and molecular relaxation at T_g. The total signal is shown in Figure 3.54 and the signals separated by a discrete Fourier transform into the reversing and non-reversing parts are shown in Figure 3.55.

The reversing part shows the glass transition and the melting as the main events. The non-reversing shows the relaxation occurring at T_g plus the cold crystallisation and the non-reversing component at T_m.

Because we may separate the events, each may be seen more clearly and measured more accurately. Heat capacity may be measured directly, and T_g separated from reactions occurring over the same temperature range, as shown in Figure 3.56.

Applications to reversible and metastable transitions of liquid crystals, or pharmaceuticals and polymers have been reported [116,117].

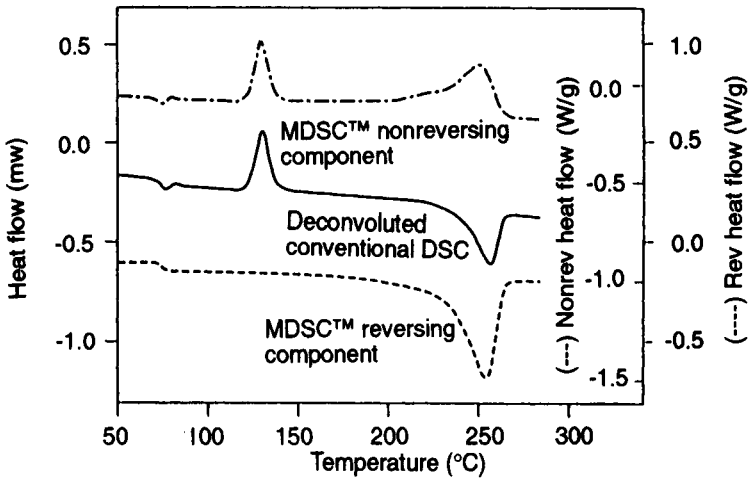

Figure 3.55 Resolved components from MDSC of PET showing the standard heat flow, reversing and non-reversing heat flows.

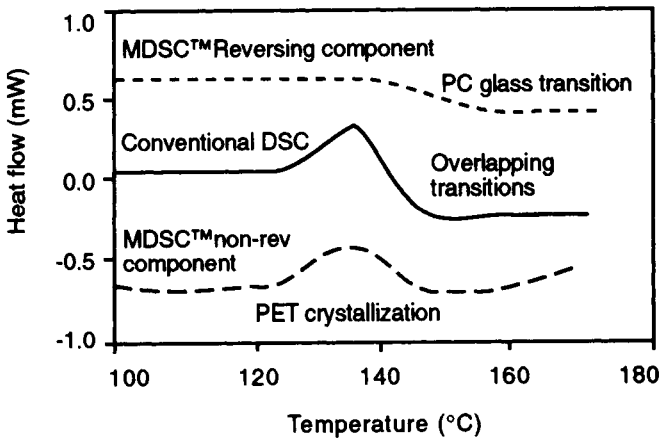

Figure 3.56 MDSC curves for a bilayer film of polycarbonate (PC) and PET. The overlap of the T_g of PC and the crystallisation exotherm of PET is resolved.

3.11 Problems

(Solutions on p. 275)

1. Which of the following changes could NOT be detected by DTA: (a) loss of moisture; (b) sublimation; (c) desorption of vapour; (d) polymer surface softening?
2. When the heating rate is changed on a DSC or DTA instrument, without changing the sensitivity, what will be the effect on: (a) the baseline; (b) any glass transition step; (c) an endothermic melting peak; (d) an exothermic reaction peak?

3. Pure naphthalene melts at 80 °C. Pure 1-naphthol melts at 123 °C. All mixtures of these two components show a *single* peak when heated and a 50 mol% mixture shows a single broad peak around 100 °C. What type of phase diagram does this suggest?
4. Pure phenacetin melts at 134.6 °C. From the DSC its heat of fusion is 53.3 kJ/mol. If the *corrected* fractions melted are 0.20 at 133.0 °C and 0.29 at 133.5 °C, estimate the purity of the phenacetin.
5. For the high-temperature reaction of copper sulphate:

$$CuSO_4 \rightarrow CuO + SO_2 + \tfrac{1}{2}O_2$$

given the data below, estimate the ΔH for this reaction and comment on the value with respect to the DTA trace given in Figure 3.36.

Compound	ΔH_f/kJ/mol at 298 K
$CuSO_4$(s)	−800
CuO(s)	−157
SO_2(g)	−297
O_2(g)	0

This estimate will be rather incorrect! Why?

6. A series of DSC runs were done on an epoxy coating material. The first, run up to 100 °C only, showed a small endothermic step at 50 °C. The second, run up to 150 °C, showed a large exothermic peak around 140 °C. The third, re-running the second material up to 200 °C, showed a smaller exothermic peak around 140 °C. The fourth showed *no* exotherm, but only an endothermic step at about 100 °C. Please explain!
7. *Without using a thermobalance*, how would you distinguish between DTA or DSC peaks that are due to structural inversions and those that are due to chemical reactions with loss of mass?
8. A mineral felspar is reported to be suspect although its chemical breakdown into Al_2O_3 and SiO_2 reveals an ideal felspar. A DTA curve shows three peaks: endothermic peaks at 600 °C and 750 °C and an exothermic peak at 990 °C. If the first and last peaks are characteristic of kaolin, $Al_2O_3 \cdot 2SiO_2 \cdot 2H_2O$, suggesting the felspar is contaminated, how would you estimate the amount of kaolin in the suspect material, given a 'pure' felspar which shows a peak at 750 °C and a pure kaolin sample?

References

1. A.L. Lavoisier, P.S. de Laplace, *Mem. R. Acad. Sci., Paris*, 1784, 355.
2. J.B. Fourier, *Theorie Analytique de la Chaleur*, Paris, 1822.
3. J.P. Joule, *Collected Works*, The Physical Society, London, 1884, p. 474.
4. J.P. McCullogh, D.W. Scott, *Experimental Thermodynamics*, Vol. 1, Butterworth, London, 1968.
5. H. Le Chatelier, *C.R. Acad. Sci., Paris*, 1887, **104**, 1443.
6. W.C. Roberts-Austen, *Proc. R. Instn. Mech. Eng.* London, 1899, p. 35.
7. E.S. Watson, M.J. O'Neill, J.Justin, N.Brenner, *Anal. Chem.*, 1964, **36**, 1233.
8. J.O. Hill, *For Better Thermal Analysis and Calorimetry* (3rd edn), ICTAC, 1991.

9. R.C. Mackenzie, *Anal. Proc.*, 1980, 217.
10. R.L. Blaine, *A Generic Definition of Differential Scanning Calorimetry*, Dupont Instruments, 1978.
11. F.E. Freeberg, T.G. Alleman, *Anal. Chem.*, 1966, **38**, 1806.
12. I. Mita, I.Imai, H.Kambe, *Thermochim. Acta*, 1971, **2**, 337.
13. H.G. Wiedemann, G. Bayer, *Thermochim. Acta*, 1985, **83**, 153.
14. P.J. Haines, G.A. Skinner, *Thermochim. Acta*, 1982, **59**, 343.
15. H.G. Wiedemann, A.Boller, *Int. Lab.*, 1992, **22**, 14.
16. *Dupont Application Brief*, No. 900B32, 1970.
17. P.J. Haines, *Educ. in Chem.*, 1969, **6**, 171.
18. R.N. Rogers, E.D. Morris, *Anal. Chem.*, 1966, **38**, 410.
19. M.E. Brown, *Introduction To Thermal Analysis*, Chapman & Hall, London, 1988.
20. C.J. Keattch, D. Dollimore, *Introduction to Thermogravimetry* (2nd edn), Heyden, London, 1975.
21. F.W. Wilburn, J.R. Hesford, J.R. Flower, *Anal. Chem.*, 1968, **40**, 777.
22. R. Melling, F.W. Wilburn, R.M. McIntosh, *Anal. Chem.*, 1969, **41**, 1275.
23. F.W. Wilburn, D. Dollimore, J.S. Crighton, *Thermochim. Acta*, 1991, **181**, 173.
24. F.W. Wilburn, D. Dollimore, J.S. Crighton, *Thermochim. Acta*, 1991, **181**, 191.
25. H.J. Borchardt, F. Daniels, *J. Amer. Chem. Soc.*, 1957, **79**, 41.
26. A.W. Coats, J.P. Redfern, *Nature*, 1964, **201**, 68.
27. M.J. Vold, *Anal. Chem.*, 1949, **21**, 683.
28. F.W. Wilburn, R.M. McIntosh, A. Turnock, *Trans. Brit. Ceram. Soc.*, 1974, **73**, 117.
29. S.L. Boersma, *J. Amer. Ceram. Soc.*, 1955, **38**, 281.
30. E.L. Charsley *et al.*, *J. Thermal Anal.*, 1993, **40**, 1415.
31. R.W. Carling, *Thermochim. Acta*, 1983, **60**, 265.
32. A.P. Gray, *Perkin-Elmer Thermal Analysis Study*, #1, Perkin-Elmer Ltd, 1972.
33. J. Pöyhönen, T. Sivonen, M. Hilpela, *Proc. 1st ICTA, Aberdeen*, Macmillan, London, 1965, p. 148.
34. Z.G. Szabo, I.K. Thege, E.E. Zapp, *Proc. 1st ESTA, Salford*, Heyden, London, 1976, p. 272.
35. W. Engel, *Explosivstoffe*, 1973, **21**, 9.
36. D. Chapman, *Chem. Rev.*, 1966, **62**, 433.
37. J.S. Aronhime, *Thermochim. Acta*, 1988, **134**, 1.
38. N.V. Lovegren, M.S. Gray, R.O. Feuge, *J. Amer. Oil Chem. Soc.*, 1976, **53**, 83.
39. E. Kaiserberger, *Thermochim. Acta*, 1989, **151**, 83.
40. J.L. Ford, P. Timmins, *Pharmaceutical Thermal Analysis*, Ellis Horwood, Chichester, 1989.
41. M.J. Hardy, *Proc 7th ICTA, Canada*, Wiley, Chichester, 1982, p. 876.
42. B. Sustar, N. Bukovec, P. Bukovec, *J. Thermal Anal.*, 1993, **40**, 475.
43. G.S. Attard, G. Williams, *Chem. in Brit.*, 1986, **22**, 919.
44. G.W. Gray, *Molecular Structure and Properties of Liquid Crystals*, Academic Press, London, 1962.
45. H.G. Wiedemann, *Mettler Application*, No. 805, 1987.
46. F.D. Ferguson, T.K. Jones, *The Phase Rule*, Butterworth, London, 1966, p. 94.
47. P. Atkins, *Physical Chemistry*, OUP, Oxford, 1978, Ch. 10.
48. E.A. Franceschi, G.A. Costa, *J. Thermal Anal.*, 1988, **34**, 451.
49. P.-Y. Chevalier, *Thermochim. Acta.*, 1989, **155**, 211.
50. A.V. Galanti, R.S. Porter, *J. Phys. Chem.*, 1972, **76**, 3089.
51. H. Jacobson, G. Reier, *J. Pharm. Sci.*, 1969, **58**, 631.
52. D.J.W. Grant, I.K.A. Abougela, G.G. Liversidge, J.M. Padfield, *Anal. Proc.*, 1982, 545 and 549.
53. F. Giordano, G.P. Bettinetti, A. La Manna, A. Marini, V. Berbenni, *J. Thermal Anal.*, 1988, **34**, 531.
54. F. Rodriguez, *Principles of Polymer Systems*, McGraw-Hill, Singapore, 1983.
55. M. Dole, *J. Polym. Sci. (C)*, 1967, **18**, 57.
56. E.M. Barrall *et al.*, *J. Appl. Polym. Sci.*, 1965, **9**, 3061.
57. M.E. Brown, *Introduction to Thermal Analysis* Chapman & Hall, London, 1988, p. 46.
58. M.J. O'Neill, *Anal. Chem.*, 1966, **38**, 1331.
59. B. Wunderlich, M. Dole, *J. Polym. Sci.*, 1957, **24**, 201.
60. B. Wunderlich, *J. Phys. Chem.*, 1965, **69**, 2078.

61. S.Z.D. Cheng, B. Wunderlich, *Thermochim. Acta*, 1988, **134**, 161.
62. A. Everett, *Materials*, Mitchells, London, 1986.
63. Mettler DSC 20 System Reference, Mettler-Toledo.
64. A.R. Ubbelohde, *Quart. Rev.*, 1957, **XI**, 246.
65. B. Wunderlich, M. Bodily, *J. Polym. Sci. (C)*, 1963, **6**, 132.
66. W.P. Brennan, *Perkin-Elmer Thermal Analysis Application Study*, 8 & 11, W.P. Brennan, Perkin-Elmer Ltd, 1973.
67. M.E. Brown, *J. Chem. Ed.*, 1979, **56**, 310.
68. P.W. Atkins, *Physical Chemistry*, OUP, Oxford, 1978, p. 219.
69. G. Widmann, O. Scherrer, *J. Thermal Anal.*, 1991, **37**, 1957.
70. S.T. Glasstone, *Textbook of Physical Chemistry* Macmillan, London, 1951, p. 650.
71. C. Plato, A.R. Glasgow, *Anal. Chem.*, 1969, **41**, 330.
72. P.D. Garn, B. Kawalec, J.J. Houser, T.F. Habash, *Proc. 7th ICTA*, Wiley, Chichester, 1982, p. 899.
73. K.E.J. Barrett, *J. Appl. Polym. Sci.*, 1967, **11**, 1617.
74. J.R. Knox, *Analytical Calorimetry* (ed. R.S. Porter, J.F. Johnson), Plenum, New York, 1968, p. 45.
75. A. Wlochowicz, M. Eder, *Thermochim. Acta*, 1988, **134**, 133.
76. ASTM E698–79: *Arrhenius Kinetic Constants for Thermally Unstable Materials*, ASTM, Philadelphia, 1979.
77. T. Ozawa, *J. Thermal Anal.*, 1970, 2, 301; 1975, 7, 601.
78. M.I. Pope, M.D. Judd, *Differential Thermal Analysis*, Heyden, London, 1977.
79. W. Wendlandt, J.P. Smith, *J. Inorg. Nucl. Chem.*, 1963, **25**, 843, 1267.
80. J.E. House, K. Farran, *J. Inorg. Nucl. Chem.*, 1972, **34**, 1466.
81. G. Beech, C.T. Mortimer, E.G. Tyler, *J. Chem. Soc.*, 1967, 925, 929.
82. R.C. Mackenzie, *Differential Thermal Analysis*, 2 Vols, Academic Press, London, 1970 and 1972.
83. *Recommendations for Testing High Alumina Cement Concrete Samples by Thermo-analytical Techniques*, Thermal Methods Group, RSC, London, 1975
84. H.G. Midgley, *Trans. Brit. Ceram. Soc.*, 1967, **66**, 161
85. J.W. Dodd, K.H. Tonge, *Thermal Methods*, ACOL, Wiley, 1987, Ch. 6.
86. R.C. Mackenzie (ed.), *The Differential Thermal Analysis of Clays*, Mineralogical Soc., London, 1957.
87. D.N. Todor, *Thermal Analysis of Minerals*, Abacus Press, Tunbridge Wells, 1976.
88. C.M. Earnest, *Thermal Analysis of Clays, Minerals and Coal*, Perkin-Elmer, Norwalk, 1984.
89. J.G. Dunn, *Stanton Redcroft Information Sheet*, No. 130, 1978.
90. J.W. Rue, W.R. Ott, *J. Thermal Anal.*, 1974, **6**, 513.
91. J.B. Farmer, A.J.D. Gilbert, P.J. Haines, *Proc. 7th ICTA*, Wiley-Heyden, Chichester, 1982, 650.
92. A.G. Sadler, W.D. Westwood, D.C. Lewis, *J. Can. Ceram. Soc.*, 1971, **21**, 127.
93. S.T. Henderson, P.W. Ranby, *J. Electrochem. Soc.*, 1951, **98**, 479.
94. M.E. Brown, R.A. Rugunanan, *Thermochim. Acta*, 1988, **134**, 413.
95. P.G. Laye, E.L. Charsley, *Thermochim. Acta*, 1987, **120**, 325.
96. T. Ozawa, *Thermochim. Acta*, 1988, **133**, 11.
97. H.-J. Chen, J.H. Sharp, *J. Thermal Anal.*, 1993, **40**, 379.
98. ASTM D 3350–84 and ASTM D 3895–80, ASTM, Philadelphia.
99. J.B. Howard, *Polym. Eng. Sci.*, 1973, **13**, 429.
100. J.M. Barton, *Advances in Polymer Science*, 1985, **72**, 111.
101. R.B. Cassel, *Perkin-Elmer Thermal Analysis Application Study*, 5, Perkin-Elmer, 1973.
102. Setaram File 10: Micro-DSC. Setaram.
103. C.F. Cullis, M.M. Hirschler, *The Combustion of Organic Polymers*, Clarendon Press, Oxford, 1981.
104. G.P. Morie, T.A. Powers, C.A. Glover, *Thermochim. Acta.* 1972, **3**, 259.
105. R.J. Seyler, *Thermochim. Acta*, 1976, **17**, 129.
106. B.Cassel, M.P. DiVito, *Int. Lab.*, 1994, **24**, 19.
107. H.G. Wiedemann, A. Boller, *Int. Lab.*, 1992, **22**, 14.
108. L.C. Thomas, *Int. Lab.*, 1987, **17**, 30.
109. *DuPont Thermal Analysis Application Briefs*, Nos 900B31 and 900B32, 1970.
110. F.R. Wright, G.W. Hicks, *Polym. Eng. Sci.*, 1978, **18**, 378.

111. G.R. Tryson, A.R. Schultz, *J. Polym. Sci., Polym. Phys. Ed.*, 1979, **17**, 2059.
112. T.R. Manley, G. Scurr, *Proc. 2nd ESTA, Aberdeen*, Heyden, London, 1981.
113. K.A. Hodd, N. Menon, *Proc. 2nd ESTA, Aberdeen*, Heyden, London, 1981.
114. P.S. Gill, S.R. Sauerbrunn, M. Reading, *J. Thermal Anal.*, 1993, **40**, 931.
115. M. Reading, D. Elliott, V.L. Hill, *J. Thermal Anal.*, 1993, **40**, 949.
116. A.F. Barnes, M.J. Hardy, T.J. Lever, *J. Thermal Anal.*, 1993, **40**, 499.
117. *TA Instruments Ltd Application Brief*, MDSC-1, 1993.

Bibliography

The general reference texts given in Chapter 1 all contain substantial sections on DTA and DSC. In addition, the following are more specific to these techniques:

R.C. Mackenzie, *Differential Thermal Analysis* (2 Vols), Academic Press, London, 1970 and 1972.
W.J. Smothers, J. Chiang, *Differential Thermal Analysis*, Chemical Publishing Co, New York, 1958.
M.I. Pope, M.D. Judd, *Differential Thermal Analysis*, Heyden, London, 1977.
J.L. McNaughton, C.T. Mortimer, *Differential Scanning Calorimetry*, Perkin-Elmer, 1975, Butterworth (Vol. 10 of IRS Physical Chemistry Series 2).
E. Kaisersberger, H. Möhler, *DSC on Polymeric Materials*, Netzsch Annual for Science and Industry, Vol. 1, 1991,
E. Kaisersberger, S. Knappe, H. Möhler, *TA for Polymer Engineering: DSC TG DMA*, Netzsch Annual, Vol. 2, 1993, Netzsch, Selb.